Electronic Supplementary Information

Contribution of Radiative Rate Constants to Crystallization-Induced Emission Enhancement in Boron-Fused Azobenzene Complexes

Masashi Nakamura[1], Masayuki Gon[1,2], and Kazuo Tanaka[1,2]*

[1] *Department of Polymer Chemistry, Graduate School of Engineering, Kyoto University, Nishikyo-ku, Katsura, Kyoto 615-8510, Japan.*

[2] *Graduate School of Global Environmental Studies, Kyoto University, Katsura, Nishikyo-ku, Kyoto 615-8510, Japan*

E-mail: tanaka@poly.synchem.kyoto-u.ac.jp

Contents page

General

^{1}H, $^{13}C\{^{1}H\}$, and $^{11}B\{^{1}H\}$ spectra were recorded on a JEOL ECZ400 instrument at 400, 100, and 128 MHz, respectively. Samples were analyzed in $CDCl_3$. The chemical shift values were expressed relative to Me_4Si for ^{1}H and $^{13}C\{^{1}H\}$ NMR as an internal standard in $CDCl_3$ and $BF_3{\cdot}Et_2O$ for $^{11}B\{^{1}H\}$ NMR as a capillary standard. Analytical thin layer chromatography (TLC) was performed with silica gel 60 Merck F254 plates. Column chromatography was performed with Wakogel® C-300 silica gel. High-resolution mass (HRMS) spectrometry was performed at the Technical Support Office (Department of Synthetic Chemistry and Biological Chemistry, Graduate School of Engineering, Kyoto University), and the HRMS spectra were obtained on a Thermo Fisher Scientific EXACTIVE spectrometer for electrospray ionization (ESI). Elemental analyses were performed at the Microanalytical Center of Kyoto University. UV–vis–NIR absorption spectra were recorded on a SHIMADZU UV-3600i plus spectrophotometer, and samples were analyzed at room temperature. Fluorescence (FL) spectra were recorded on a HORIBA Scientific Fluorolog-3 spectrofluorometer with PMT P928 as detectors. FL spectra measurement at 77 K was conducted by Oxford Optistat DN2 by cooling with liquid N_2. An absolute FL quantum yield (Φ_{FL}) was recorded on a Hamamatsu Photonics Quantaurus-QY Plus C13534-01 with an integral sphere without re-absorption corrections.[1] The measurement at 77 K was performed in a dewar quartz flask with an integral sphere by cooling with liquid N_2. The data were collected at least 5 times, and it was confirmed that the error was within 10%, then we calculated the average values. A FL lifetime measurement was performed on a Horiba FluoreCube spectrofluorometer system; excitation was carried out using UV and visible diode lasers (NanoLED: N-375L (369 and 375 nm, Pulse width < 200 ps, 28 pJ/pulse). The measurement at 77 K was conducted by Oxford Optistat DN2 by cooling with liquid N_2. The data were collected several times and we adopted them with the lowest χ parameters (the best fitting data). Powder X-ray diffraction (PXRD) data were collected with a Rigaku SmartLab Diffractometer (sealed tube (50 kV, 40 mA); Cu Kα, 1.542 Å; Bragg–Brentano geometry, a HyPix-3000 detector). X-ray crystallographic analysis was carried out by a Rigaku Saturn 724+ with MicroMax-007 HF CCD diffractometer with Varimax Mo optics using graphite-monochromated MoKα radiation. A symmetry-related absorption correction was carried out by using the program REQAB.[2] The structures were solved with SHELXT 2018/2[3,4] and refined on F^2 with SHELXL 2018/3[3,5,6] on Yadokari-XG.[7] All hydrogen atoms were placed at calculated positions and refined using a riding model. The program ORTEP-3[8] was used to generate the X-ray structural diagram. All of the crystal diagrams were visualized with Mercury.[9] The program Multiwfn 3.8[10] was used to conduct the independent gradient model based on Hirshfeld partition of molecular density (IGMH) analysis.[11] The results of the IGMH analysis were visualized by Visual Molecular Dynamics 1.9.3 (VMD).[12]

Materials

Commercially available compounds used without purification:

Boron trifluoride diethyl etherate (≥46% BF_3 basis) ($BF_3 \cdot Et_2O$) (Sigma-Aldrich Co. LLC.)

Commercially available solvents:

toluene (deoxidized grade, FUJIFILM Wako Pure Chemical Corporation)

triethylamine (NEt_3) (Kanto Chemical Co., Inc.) purified by passage through solvent purification columns under N_2 pressure.[13]

Compounds prepared as described in the literatures:

4,4′-(Diazene-1,2-diyl)bis(1-fluoro-3-hydroxybenzene) (**AzOH-F**) [14]

4,4′-(Diazene-1,2-diyl)bis(1-chloro-3-hydroxybenzene) (**AzOH-Cl**) [15]

BAz-H [16]

BAz-Br [16]

Synthetic Procedures and Characterization

Synthesis of BAz-F

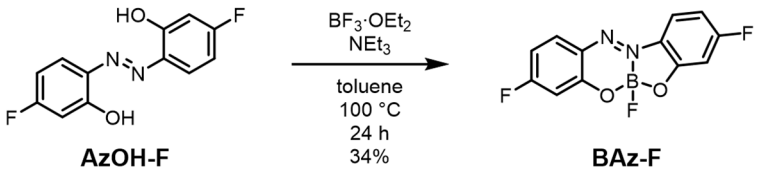

AzOH-F (500 mg, 2.00 mmol) was placed in a round-bottom flask equipped with a magnetic stirring bar. After degassing and filling N_2 three times, toluene (20 mL) was added to the flask. $BF_3{\cdot}Et_2O$ (1.26 mL, 10.0 mmol) and NEt_3 (0.70 mL, 5.00 mmol) were added to the mixture. After finishing the addition, the reaction was carried out at 100 °C for 24 h. After the reaction, silica gel was added to the solution, the solvent was removed with a rotary evaporator, and then purified with column chromatography on SiO_2 (hexane/CH_2Cl_2 = 3/2 v/v as an eluent). Further purification was carried out by recrystallization with acetonitrile to afford **BAz-F** (198 mg, 0.686 mmol, 34%) as an orange crystal.

R_f = 0.44 (hexane/CH_2Cl_2 = 3/2 v/v). ^{1}H NMR ($CDCl_3$, 400 MHz) δ 8.01–7.97 (m, 1H), 7.82 (dd, J = 9.2, 5.0 Hz, 1H), 7.02–6.98 (m, 2H), 6.92 (dd, J = 9.2, 2.3 Hz, 1H), 6.84 (td, J = 9.1, 2.3 Hz, 1H) ppm; ^{13}C{^{1}H} NMR ($CDCl_3$, 100 MHz) δ 168.3 (d, $J_{C\text{-}F}$ = 259.7 Hz), 168.3 (d, $J_{C\text{-}F}$ = 259.7 Hz), 162.5 (d, $J_{C\text{-}F}$ = 14.4 Hz), 148.3 (d, $J_{C\text{-}F}$ = 14.4 Hz), 136.8, 133.6 (d, $J_{C\text{-}F}$ = 12.5 Hz), 129.0, 118.2 (d, $J_{C\text{-}F}$ = 11.5 Hz), 111.7 (d, $J_{C\text{-}F}$ = 24.0 Hz), 110.4 (d, $J_{C\text{-}F}$ = 25.9 Hz), 107.3 (d, $J_{C\text{-}F}$ = 24.9 Hz), 103.9 (d, $J_{C\text{-}F}$ = 26.8 Hz) ppm; ^{11}B{^{1}H} NMR ($CDCl_3$, 128 MHz) δ 1.49 (d, J = 34.2 Hz) ppm. HRMS (ESI) calcd. for $C_{12}H_6N_2F_3BO_2$ $[M]^-$: 278.0480, found: 278.0477. Elemental analysis calcd. for $C_{12}H_6BF_3N_2O_2$: C 51.85 H 2.18 N 10.08, found: C 51.88 H 2.16 N 10.17.

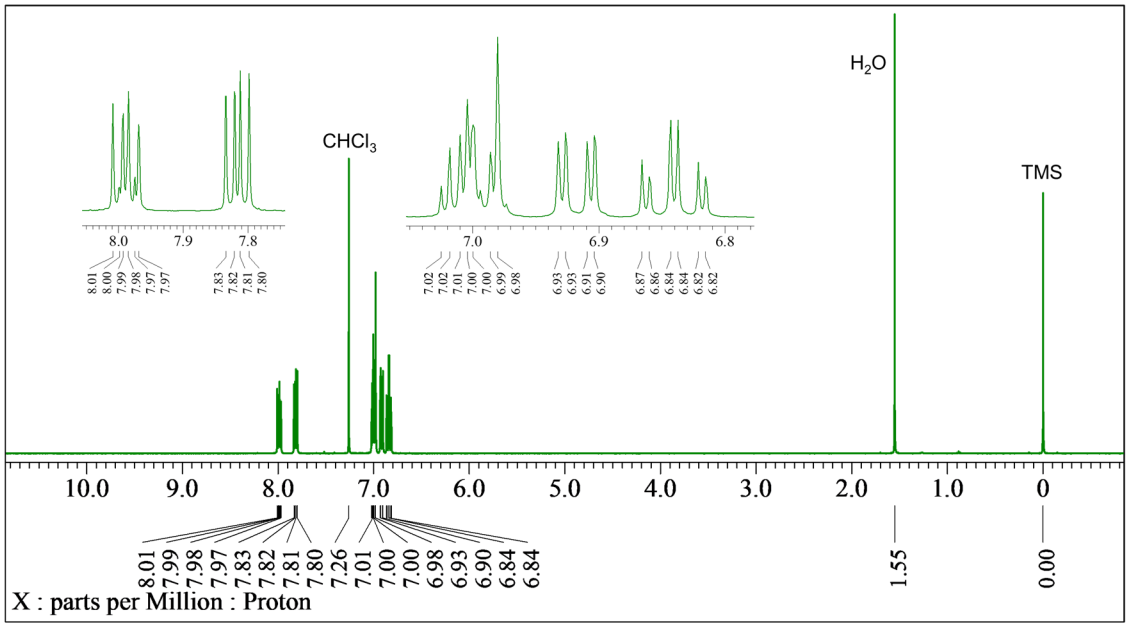

Chart S1. ^{1}H NMR spectrum of **BAz-F** in $CDCl_3$, 400 MHz.

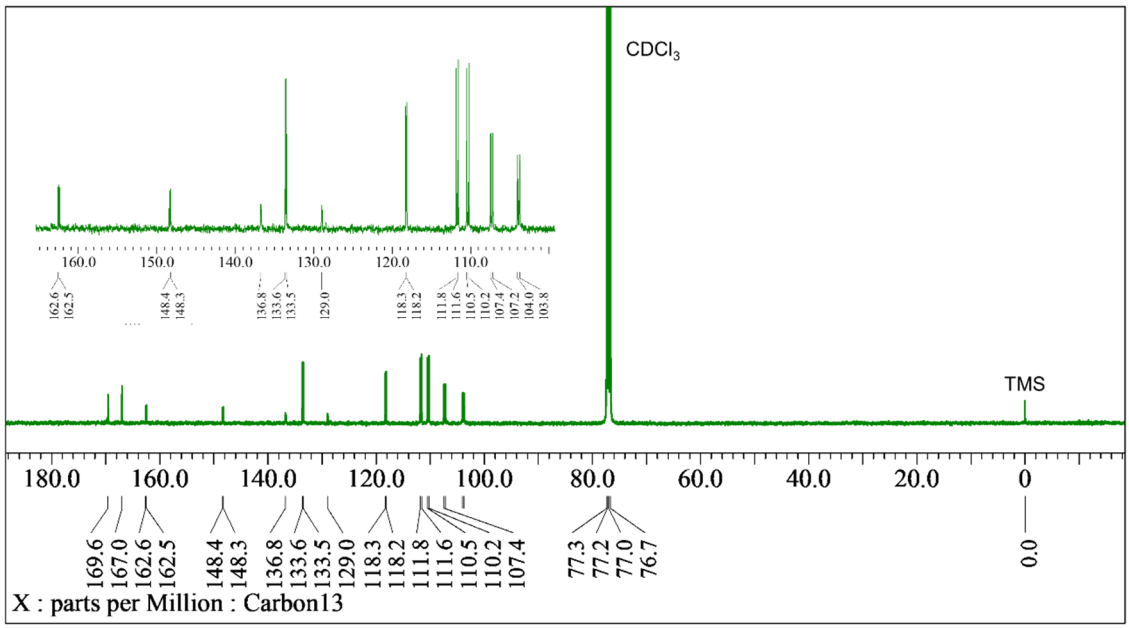

Chart S2. $^{13}C\{^{1}H\}$ NMR spectrum of **BAz-F** in $CDCl_3$, 100 MHz.

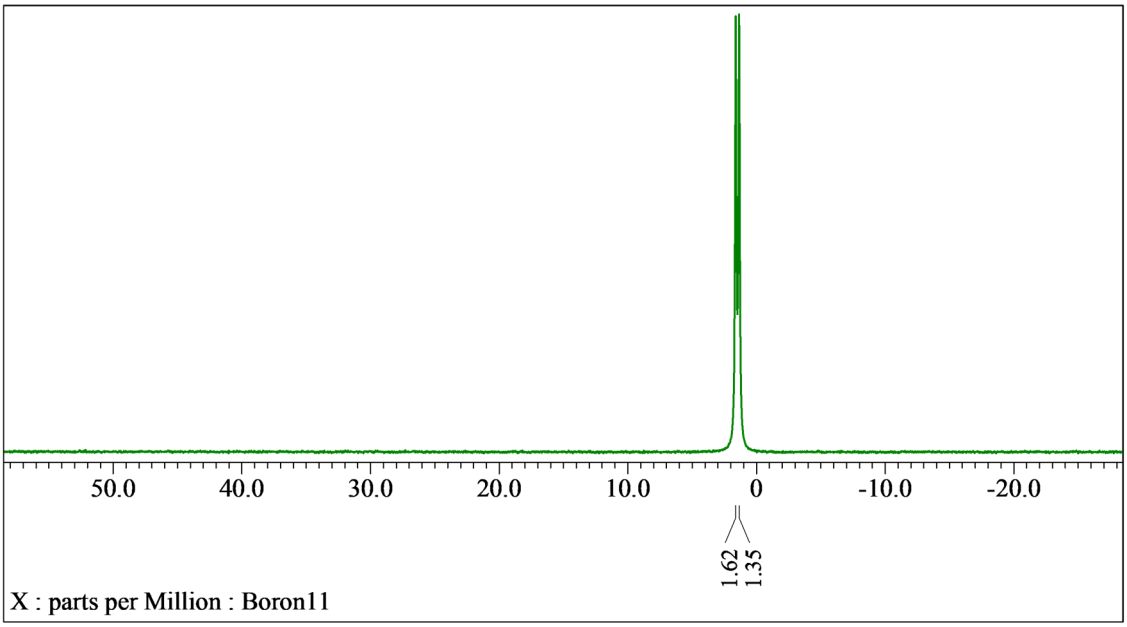

Chart S3. $^{11}B\{^{1}H\}$ NMR spectrum of **BAz-F** in $CDCl_3$, 128 MHz.

Synthesis of BAz-Cl

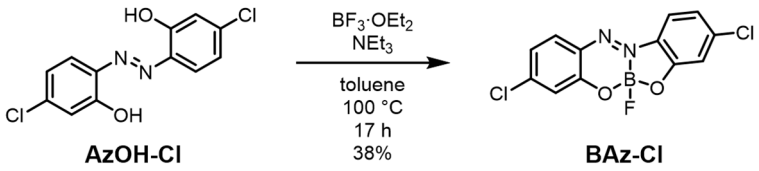

AzOH-Cl (142 mg, 0.500 mmol) was placed in a round-bottom flask equipped with a magnetic stirring bar. After degassing and filling N_2 three times, toluene (10 mL) was added to the flask. $BF_3{\cdot}Et_2O$ (0.31 mL, 2.50 mmol) and NEt_3 (0.17 mL, 1.25 mmol) were added to the mixture. After finishing the addition, the reaction was carried out at 100 °C for 17 h. After the reaction, silica gel was added to the solution, the solvent was removed with a rotary evaporator, and then purified with column chromatography on SiO_2 (hexane/CH_2Cl_2 = 2/1 v/v as an eluent). Further purification was carried out by recrystallization with hexane to afford **BAz-Cl** (59 mg, 0.189 mmol, 38%) as a red crystal.

R_f = 0.43 (hexane/CH_2Cl_2 = 2/1 v/v). ^{1}H NMR ($CDCl_3$, 400 MHz) δ 7.91 (d, J = 8.7 Hz, 1H), 7.75 (d, J = 8.7 Hz, 1H), 7.33 (d, J = 1.8 Hz, 1H), 7.24 (d, J = 2.3 Hz, 1H), 7.24 (dd, J = 8.7, 2.3 Hz, 1H), 7.10 (dd, J = 8.7, 1.8 Hz, 1H) ppm; ^{13}C{^{1}H} NMR ($CDCl_3$, 100 MHz) δ 161.6, 146.8, 144.5, 143.5, 138.4, 132.3, 131.1, 123.9, 122.9, 120.9, 117.6, 116.9 ppm; ^{11}B{^{1}H} NMR ($CDCl_3$, 128 MHz) δ 1.43 (d, J = 34.2 Hz). HRMS (ESI) calcd. for $C_{12}H_6N_2FCl_2BO_2$ $[M]^-$: 309.9889, found: 309.9888. Elemental analysis calcd. for $C_{12}H_6BCl_2FN_2O_2$: C 46.36 H 1.95 N 9.01, found: C 46.08 H 1.99 N 8.96.

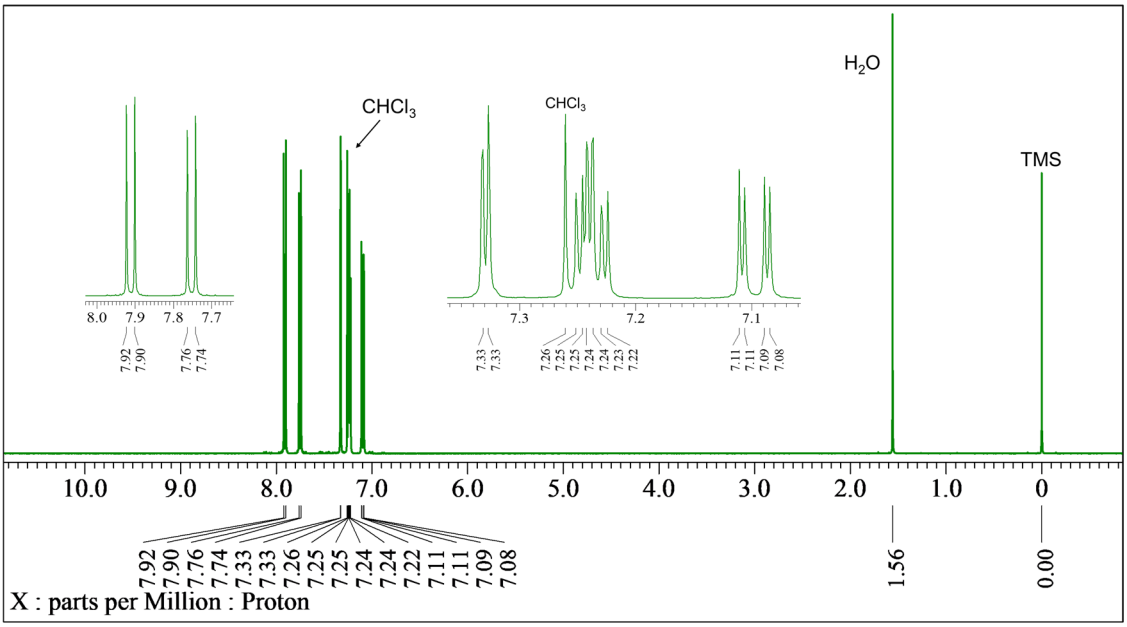

Chart S4. ^{1}H NMR spectrum of **BAz-Cl** in $CDCl_3$, 400 MHz.

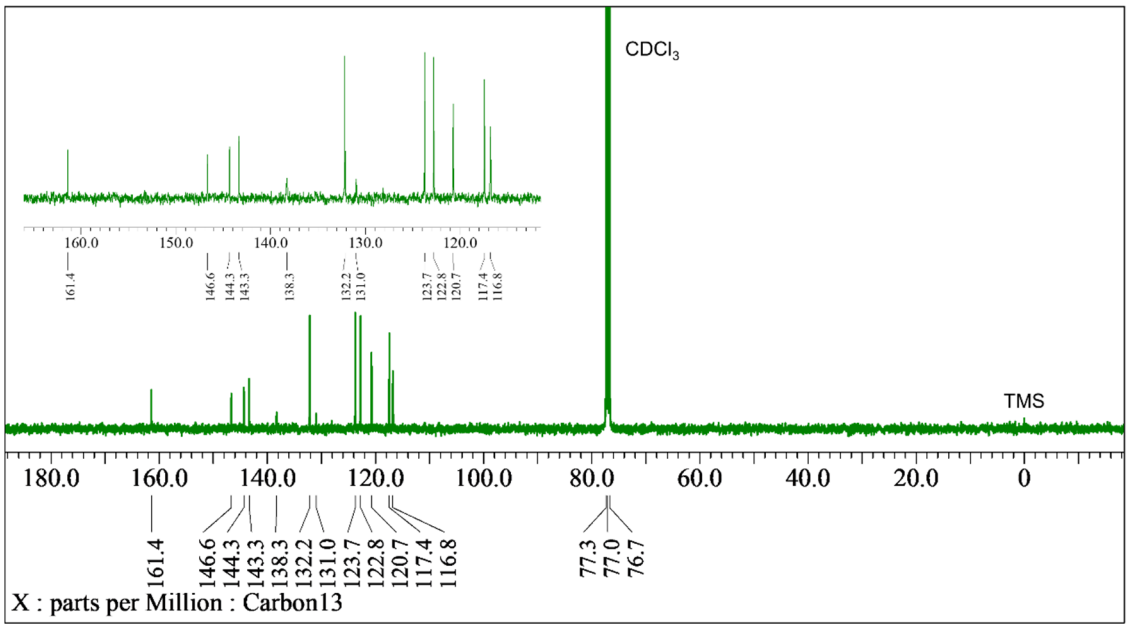

Chart S5. $^{13}C\{^{1}H\}$ NMR spectrum of **BAz-Cl** in $CDCl_3$, 100 MHz.

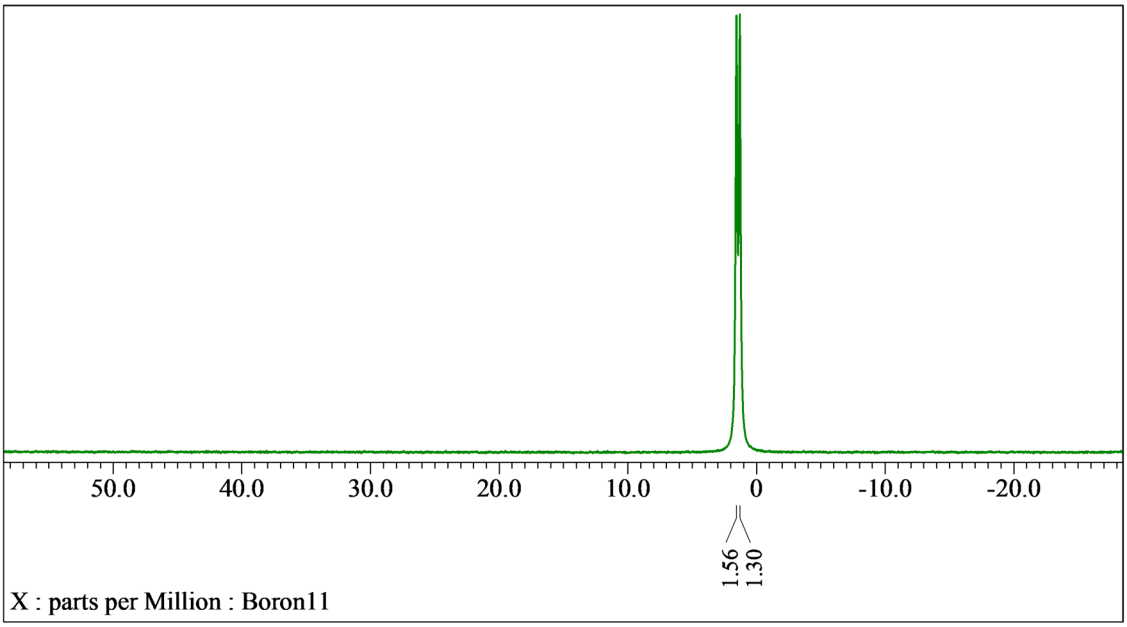

Chart S6. $^{11}B\{^{1}H\}$ NMR spectrum of **BAz-Cl** in $CDCl_3$, 128 MHz.

Single crystal X-ray structures

Table S1. Crystallographic data of **BAz-H** (CCDC:2302562)

Empirical formula	$C_{12}H_8BFN_2O_2$
Formula weight	242.01
Temperature (K)	143(2)
Wavelength (Å)	0.71075
Crystal system, space group	Monoclinic, $P\ 2_1/c$
Unit cell dimensions	a=6.982(4)
	b=21.445(11)
	c=7.808(4)
	α=90
	β=114.861(7)
	γ=90
Volume (Å^3)	1060.7(10)
Z, calculated density (g cm^{-3})	4, 1.515
Absorption coefficient	0.115
F(000)	496
Crystal size (mm)	0.17 × 0.10 × 0.04
θ range for data collection	3.028–27.512
Limiting indices	$-9\leq h\leq 9$, $-25\leq k\leq 27$, $-10\leq l\leq 9$
Reflections collected (unique)	2394/1272 [R(int)=0.1066]
Completeness to theta	0.981
Max. and min. transmission	1.000, 0.617
Goodness-of-fit on F^2	0.805
Final R indices [$I > 2\sigma(I)$][a]	R_1 = 0.0513, wR_2 = 0.0808
R indices (all data)	R_1 = 0.1016, wR_2 = 0.1117

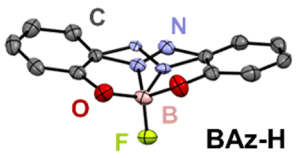

[a] $R_1 = \Sigma(|F_0|-|F_c|)/\Sigma|F_0|$. w$R_2 = [\Sigma w(F^2_0-F^2_c)^2/\Sigma w(F^2_0)^2]^{1/2}$. $w = 1/[\sigma^2(F^2_0)+[(ap)^2+bp]]$, where $p = [\max(F^2_0,0)+{}^2F^2_c]/3$.

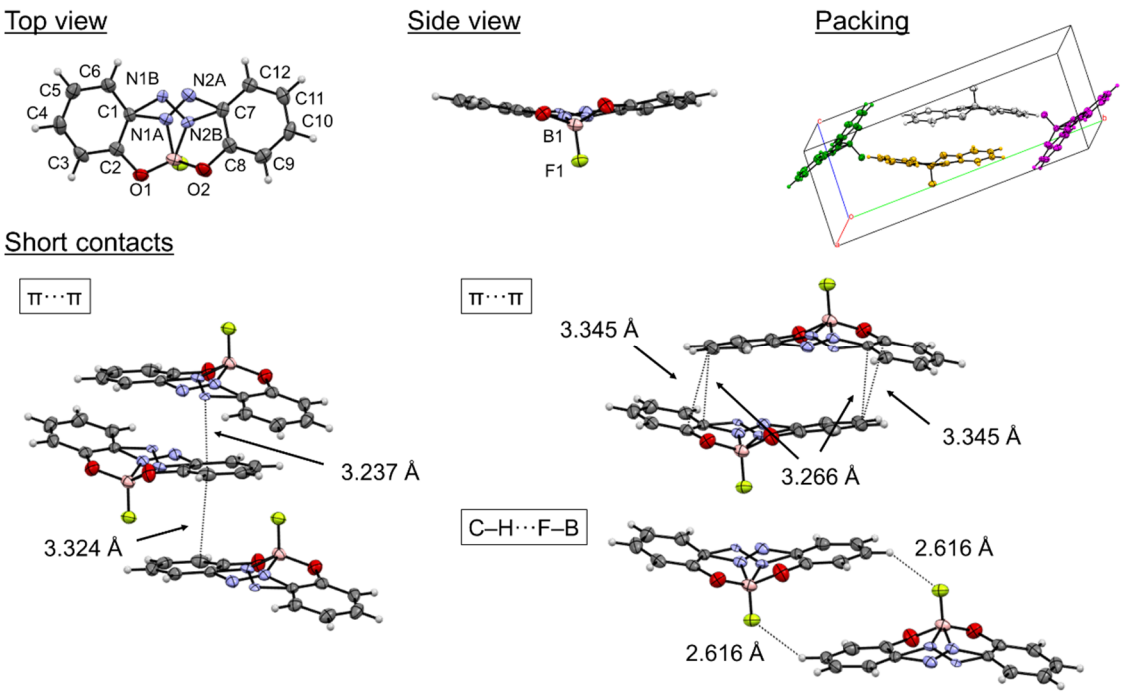

Figure S1. ORTEP drawings, packing diagrams (color: symmetry operation), and the surrounding interactions of **BAz-H**. Thermal ellipsoids are scaled to the 50% probability level. A short contact indicates that the distance between a couple of atoms less than sum of their van der Waals radii. All of the diagrams were visualized with Mercury.[9]

Table S2. Crystallographic data of **BAz-F** (CCDC:2302563)

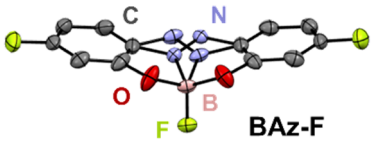

Empirical formula	$C_{12}H_6BF_3N_2O_2$
Formula weight	278.00
Temperature (K)	143(2)
Wavelength (Å)	0.71075
Crystal system, space group	Monoclinic, *C* 2/c
Unit cell dimensions	a=21.821(14)
	b=6.154(3)
	c=18.764(12)
	α=90
	β=120.182(8)
	γ=90
Volume (Å^3)	2178(2)
Z, calculated density (g cm^{-3})	8, 1.696
Absorption coefficient	0.150
F(000)	1120
Crystal size (mm)	0.14 × 0.11 × 0.02
θ range for data collection	3.482–27.478
Limiting indices	$-28\leq h\leq 28$, $-7\leq k\leq 7$, $-17\leq l\leq 24$
Reflections collected (unique)	2490/1196 [*R*(int)=0.0799]
Completeness to theta	0.998
Max. and min. transmission	1.000, 0.708
Goodness-of-fit on F^2	0.735
Final *R* indices [$I > 2\sigma(I)$][a]	R_1 = 0.0439, wR_2 = 0.0802
R indices (all data)	R_1 = 0.0910, wR_2 = 0.1003

[a] $R_1 = \Sigma(|F_0|-|F_c|)/\Sigma|F_0|$. w$R_2 = [\Sigma w(F^2_0-F^2_c)^2/\Sigma w(F^2_0)^2]^{1/2}$. $w = 1/[\sigma^2(F^2_0)+[(ap)^2+bp]]$, where $p = [\max(F^2_0,0)+{}^2F^2_c]/3$.

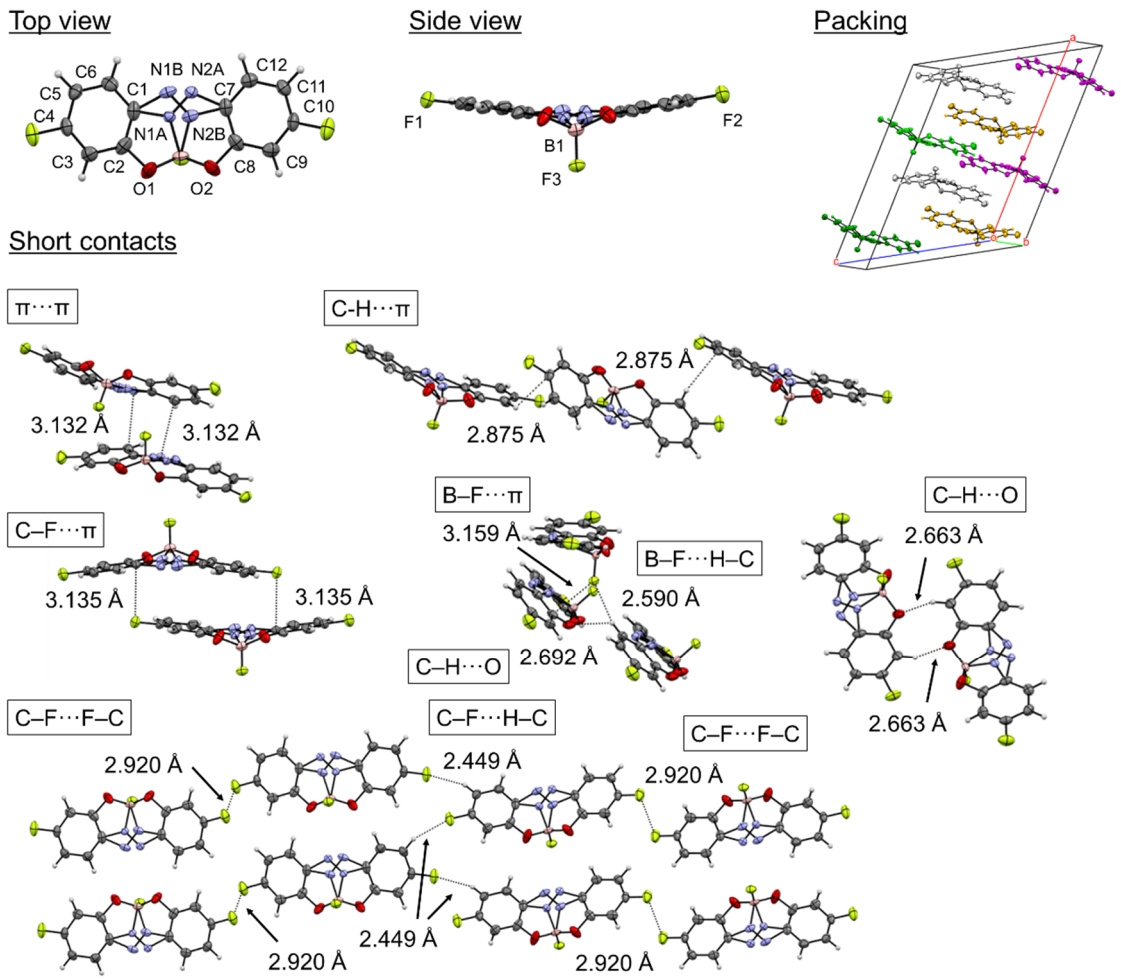

Figure S2. ORTEP drawings, packing diagrams (color: symmetry operation), and the surrounding interactions of **BAz-F**. Thermal ellipsoids are scaled to the 50% probability level. A short contact indicates that the distance between a couple of atoms less than sum of their van der Waals radii. All of the diagrams were visualized with Mercury.[9]

Table S3. Crystallographic data of **BAz-Cl** (CCDC:2302564)

Empirical formula	$C_{12}H_6BCl_2FN_2O_2$
Formula weight	310.90
Temperature (K)	143(2)
Wavelength (Å)	0.71075
Crystal system, space group	Triclinic, $P\,\bar{1}$
Unit cell dimensions	a=7.084(4)
	b=7.205(5)
	c=13.827(7)
	α=96.26(3)
	β=97.76(5)
	γ=116.43(2)
Volume (Å^3)	614.7(6)
Z, calculated density (g cm^{-3})	2, 1.680
Absorption coefficient	0.540
F(000)	312
Crystal size (mm)	0.11 × 0.07 × 0.03
θ range for data collection	3.029–27.460
Limiting indices	$-9\le h\le 9$, $-9\le k\le 9$, $-14\le l\le 17$
Reflections collected (unique)	2696/1707 [R(int)=0.0481]
Completeness to theta	0.957
Max. and min. transmission	1.000, 0.705
Goodness-of-fit on F^2	0.981
Final R indices [$I > 2\sigma(I)$][a]	R_1 = 0.0544, wR_2 = 0.0965
R indices (all data)	R_1 = 0.0980, wR_2 = 0.1132

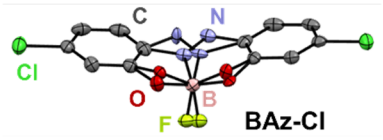

[a] $R_1 = \Sigma(|F_0|-|F_c|)/\Sigma|F_0|$. w$R_2 = [\Sigma w(F^2_0-F^2_c)^2/\Sigma w(F^2_0)^2]^{1/2}$. $w = 1/[\sigma^2(F^2_0)+[(ap)^2+bp]]$, where $p = [\max(F^2_0,0)+{}^2F^2_c]/3$.

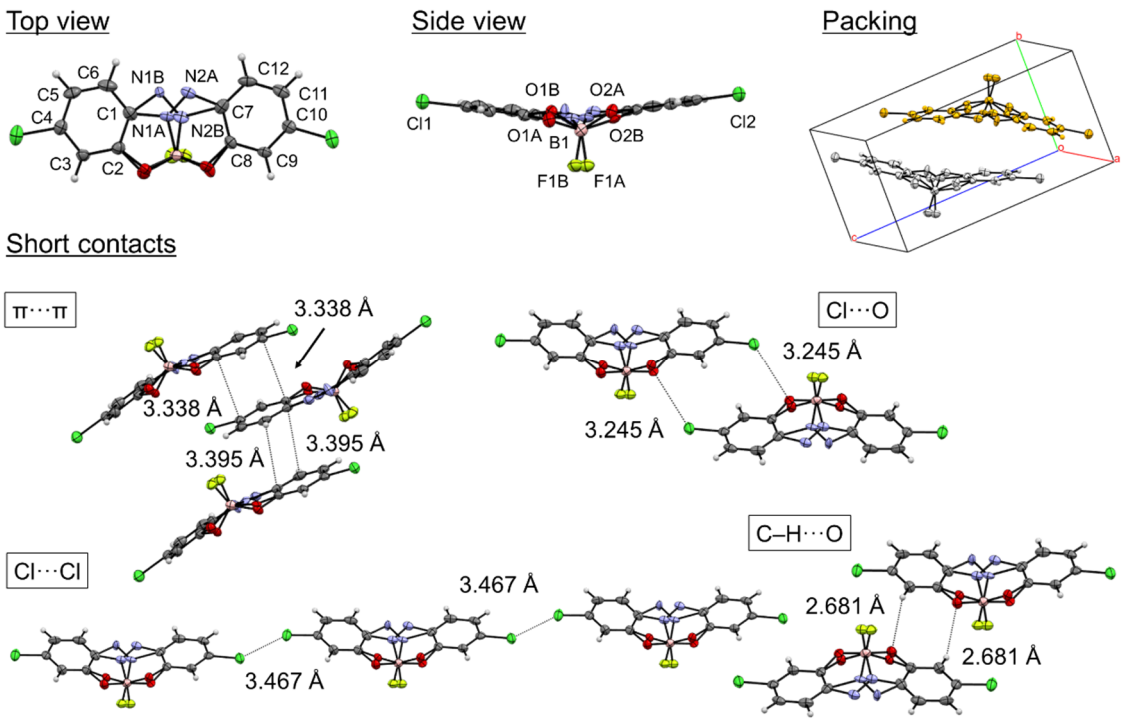

Figure S3. ORTEP drawings, packing diagrams (color: symmetry operation), and the surrounding interactions of **BAz-Cl**. Thermal ellipsoids are scaled to the 50% probability level. A short contact indicates that the distance between a couple of atoms less than sum of their van der Waals radii. All of the diagrams were visualized with Mercury.[9]

Table S4. Crystallographic data of **BAz-Br** (CCDC: 2339632)

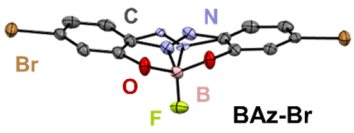

Empirical formula	$C_{12}H_6BBr_2FN_2O_2$
Formula weight	399.82
Temperature (K)	143(2)
Wavelength (Å)	0.71075
Crystal system, space group	Triclinic, *P* -1
Unit cell dimensions	a=6.975(3)
	b=7.306(3)
	c=14.302(6)
	α=95.261(3)
	β=97.928(6)
	γ=115.739(7)
Volume (Å^3)	640.8(5)
Z, calculated density (g cm^{-3})	2, 2.072
Absorption coefficient	6.337
F(000)	384
Crystal size (mm)	0.10 × 0.03 × 0.01
θ range for data collection	3.141–27.506
Limiting indices	$-9\leq h\leq 7$, $-8\leq k\leq 9$, $-18\leq l\leq 18$
Reflections collected (unique)	2802/2074 [*R*(int)=0.0277]
Completeness to theta	0.954
Max. and min. transmission	1.000, 0.777
Goodness-of-fit on F^2	0.978
Final *R* indices [$I > 2\sigma(I)$][a]	R_1 = 0.0334, wR_2 = 0.0623
R indices (all data)	R_1 = 0.0517, wR_2 = 0.0669

[a] $R_1 = \Sigma(|F_0|-|F_c|)/\Sigma|F_0|$. w$R_2 = [\Sigma w(F^2_0-F^2_c)^2/\Sigma w(F^2_0)^2]^{1/2}$. $w = 1/[\sigma^2(F^2_0)+[(ap)^2+bp]]$, where $p = [\max(F^2_0,0)+{}^2F^2_c]/3$.

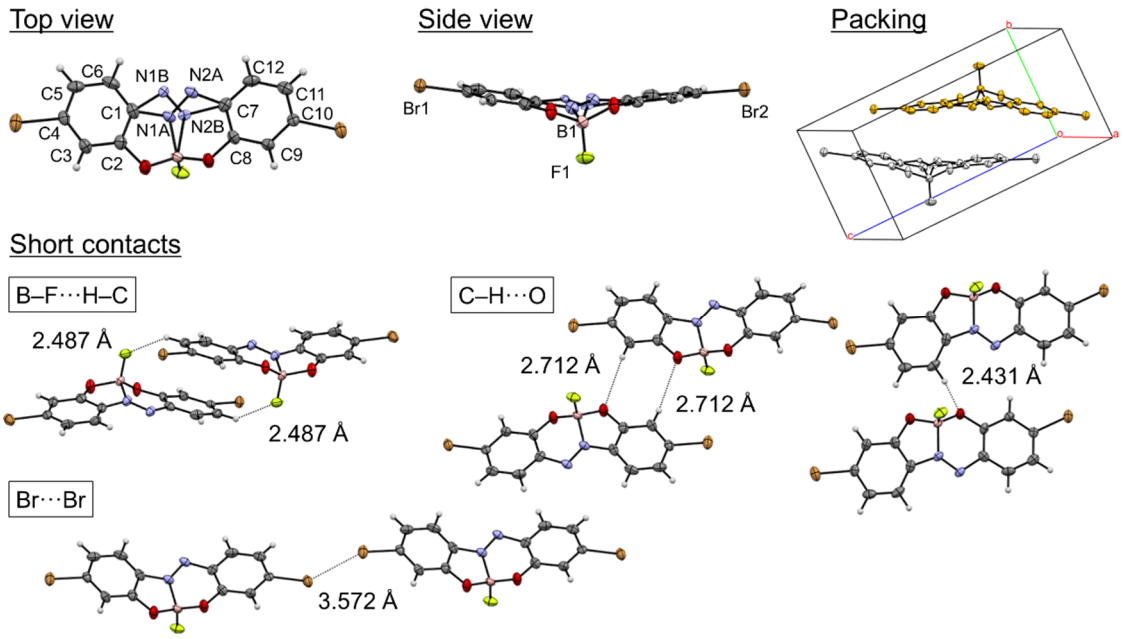

Figure S4. ORTEP drawings, packing diagrams (color: symmetry operation), and the surrounding interactions of **BAz-Br**. Thermal ellipsoids are scaled to the 50% probability level. A short contact indicates that the distance between a couple of atoms less than sum of their van der Waals radii. All of the diagrams were visualized with Mercury.[9]

Powder X-ray diffraction

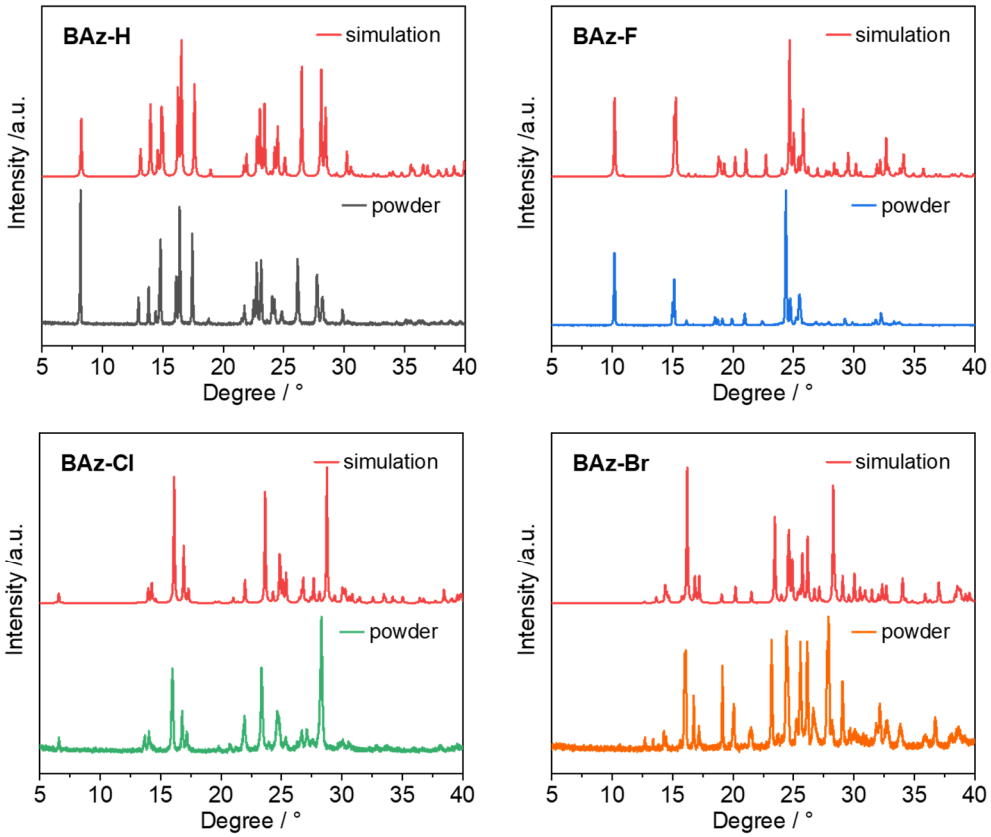

Figure S5. Simulated and experimental PXRD patterns of BAz derivatives.

Optical properties at room temperature

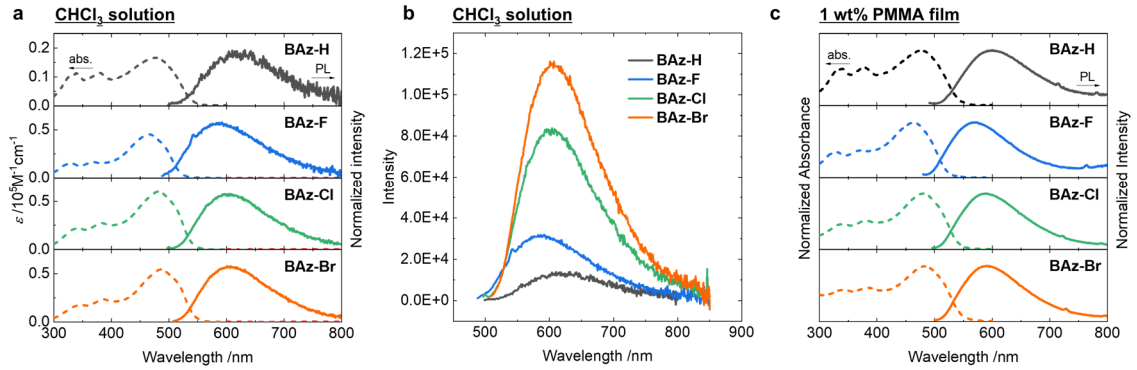

Figure S6. (a) UV–vis–NIR absorption spectra, normalized FL spectra, and (b) FL spectra in chloroform (1.0×10^{-5} M). (c) Normalized UV–vis–NIR absorption and normalized FL spectra in 1 wt% PMMA dispersed films.

Table S5. Spectroscopic data of BAz derivatives at room temperature

		λ_{abs} /nm	ε /10^5 cm^{-1} M^{-1}	λ_{FL} [a] /nm	ν [b] /cm^{-1}
BAz-H	$CHCl_3$ (1.0×10^{-5} M)	477	0.166	624	4940
	1 wt% PMMA Film	476	–[f]	599	4310
	Crystal	472	–[f]	618	5000
BAz-F	$CHCl_3$ (1.0×10^{-5} M)	465	0.454	592	4610
	1 wt% PMMA Film	465	–[f]	568	3900
	Crystal	458	–[f]	584	4710
BAz-Cl	$CHCl_3$ (1.0×10^{-5} M)	482	0.601	604	4190
	1 wt% PMMA Film	481	–[f]	587	3750
	Crystal	539	–[f]	645	3050
BAz-Br	$CHCl_3$ (1.0×10^{-5} M)	486	0.544	607	4100
	1 wt% PMMA Film	485	–[f]	589	3640
	Crystal	546	–[f]	652	2980

		Φ_{FL} [c] /%	τ [d] /ns (α)	k_r [e] /10^8 s^{-1}	k_{nr} [e] /10^8 s^{-1}
BAz-H	$CHCl_3$ (1.0×10^{-5} M)	–[f]	–[f]	–[f]	–[f]
	1 wt% PMMA Film	0.8	0.31 (42%) 0.02 (20%) 1.0 (38%)	0.15	19
	Crystal	6.1	0.16 (38%) 1.4 (62%)	0.68	10

BAz-F	$CHCl_3$ (1.0×10^{-5} M)	–[f]	–[f]	–[f]	–[f]
	1 wt% PMMA Film	0.6	0.44 (41%)	0.08	13
			0.08 (25%)		
			1.6 (34%)		
	Crystal	17.1	0.43 (17%)	1.1	5.4
			1.8 (83%)		
BAz-Cl	$CHCl_3$ (1.0×10^{-5} M)	–[f]	–[f]	–[f]	–[f]
	1 wt% PMMA Film	1.5	0.54 (50%)	0.20	13
			0.12 (20%)		
			1.5 (30%)		
	Crystal	11.5	0.34 (28%)	1.3	10
			1.1 (72%)		
BAz-Br	$CHCl_3$ (1.0×10^{-5} M)	–[f]	–[f]	–[f]	–[f]
	1 wt% PMMA Film	2.3	0.51 (47%)	0.30	13
			0.08 (16%)		
			1.4 (378%)		
	Crystal	6.7	0.34 (53%)	1.2	17
			0.80 (47%)		

[a] Excited at λ_{abs}; [b] Approximate value of Stokes shift, $\nu = (1 / \lambda_{abs} - 1 / \lambda_{FL}) \times 10^7$, because just converting the wavelength to the wavenumber and using the different instruments to measure the UV absorption and PL spectra might generate errors of the true value of Stokes shift.[17]; [c] Absolute FL quantum yield, excited at λ_{abs}; [d] FL lifetime, excited at 375 nm (for 1 wt% PMMA films) and 369 nm (for crystals) LED lasers, monitored at λ_{FL}. The IRF full width at half maximum (FWHM) value is probably higher than the shortest lifetime component among the multiple lifetime components. The shortest lifetime component is acceptable in the fitting results if the time-correlated single photon counting (TCSPC) data are analyzed with multiexponential fits including the short and long lifetime components. However, it is noted that the analysis of the short time components may contain errors.; [e] $k_r = \Phi_{FL} / \tau_{av}$, $k_{nr} = (1 - \Phi_{FL}) / \tau_{av}$, $\tau_{av} = \Sigma \alpha_i \tau_i$, α: relative amplitude. The analysis was conducted by using the average lifetime (τ_{av}) assuming that the emission was from a single state with Φ_{FL}.; [f] Not detected.

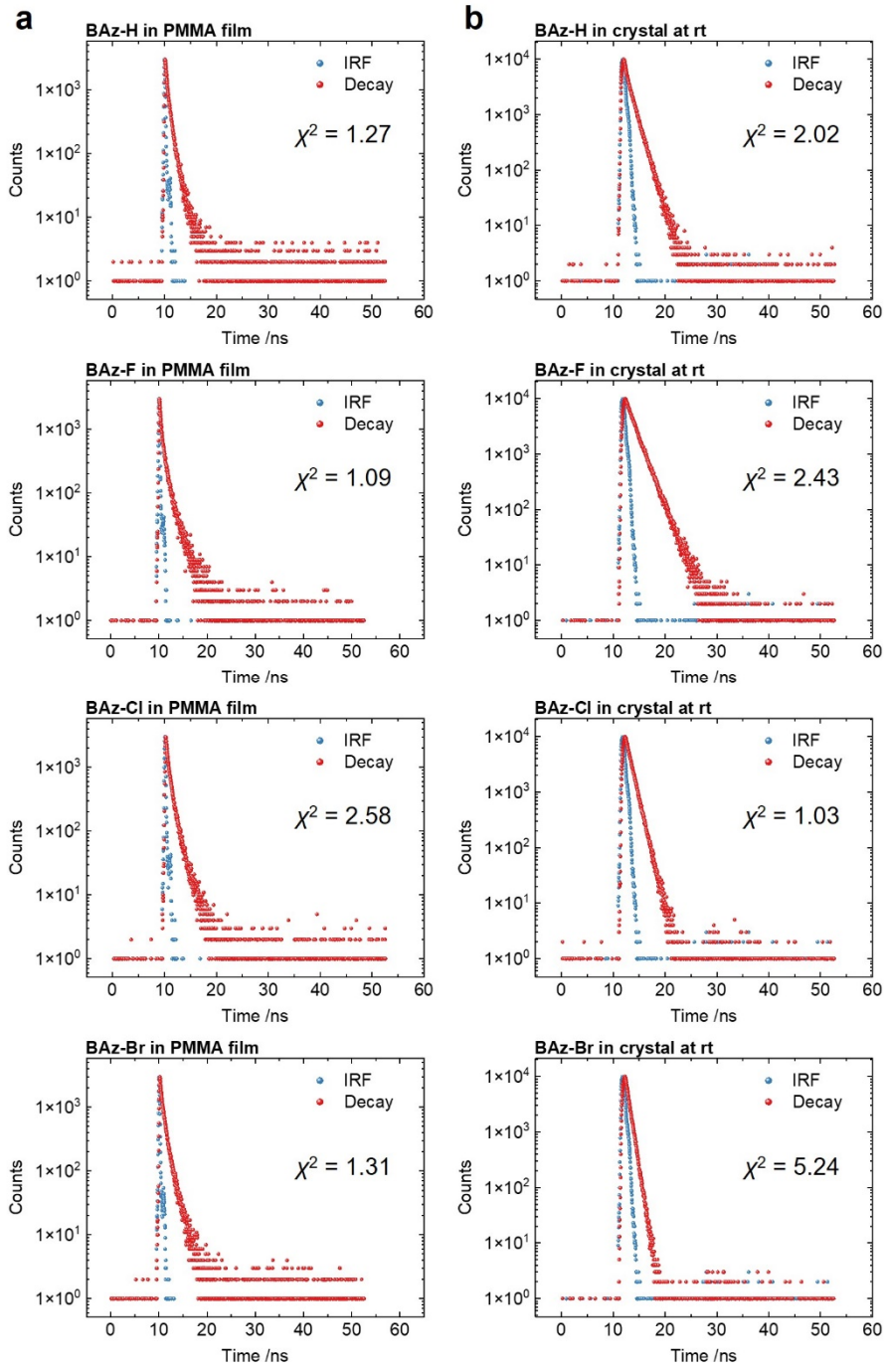

Figure S7. FL lifetime decay curves in (a) 1 wt% PMMA dispersed film (excited at 375 nm with an LED laser) and (b) crystal (excited at 369 nm with an LED laser) at room temperature. Their emissions at the FL peak tops were monitored. The performance of each laser slightly differs. For the purpose of accurate measurement, we used the laser with the narrower pulse width if the lifetime decay curves contained the components with a short fluorescence lifetime.

Optical properties at 77 K

Table S6. Spectroscopic data of BAz derivatives at 77 K

		λ_{ex} [a] /nm	λ_{FL} [b] /nm	Φ_{FL} [c] /%	τ [d] /ns (α)	k_r [e] /10^8 s^{-1}	k_{nr} [e] /10^8 s^{-1}
BAz-H	2MeTHF	477	599	19.2	1.4 (19%)	0.61	2.6
	(1.0×10^{-5} M)				3.6 (81%)		
	Tol/2MP = 1/9	477	591	24.8	2.1 (19%)	0.63	1.9
	(1.0×10^{-5} M)				4.4 (81%)		
	Crystal	472	605	26.7	3.4 (43%)	0.55	1.8
					5.4 (57%)		
BAz-F	2MeTHF	464	573	45.6	3.0 (13%)	0.83	1.0
	(1.0×10^{-5} M)				5.8 (87%)		
	Tol/2MP = 1/9	465	576	54.0	2.5 (7%)	0.87	0.74
	(1.0×10^{-5} M)				6.5 (93%)		
	Crystal	458	572	57.4	2.9 (50%)	1.4	1.1
					5.2 (50%)		
BAz-Cl	2MeTHF	481	585	54.6	2.3 (9%)	1.1	0.92
	(1.0×10^{-5} M)				5.2 (91%)		
	Tol/2MP = 1/9	482	589	58.7	3.3 (9%)	1.0	0.73
	(1.0×10^{-5} M)				5.9 (91%)		
	Crystal	539	626	34.2	2.0 (93%)	1.7	3.2
					3.0 (7%)		
BAz-Br	2MeTHF	485	592	53.3	2.1 (7%)	1.3	1.1
	(1.0×10^{-5} M)				4.3 (93%)		
	Tol/2MP = 1/9	485	589	47.3	1.7 (7%)	1.2	1.3
	(1.0×10^{-5} M)				4.3 (93%)		
	Crystal	546	631	19.6	1.1	1.9	7.7

Tol = toluene, 2MP = 2-methylpentane; [a] The longest absorption maximum in each state measured at room temperature; [b] Excited at λ_{ex}; [c] Absolute FL quantum yield, excited at λ_{ex}; [d] FL lifetime, excited at 369 nm LED lasers, monitored at λ_{FL}; [e] $k_r = \Phi_{FL} / \tau_{av}$, $k_{nr} = (1 - \Phi_{FL}) / \tau_{av}$, $\tau_{av} = \Sigma\alpha_i\tau_i$, α: relative amplitude. The analysis was conducted by using the average lifetime (τ_{av}) assuming that the emission was from a single state with Φ_{FL}.

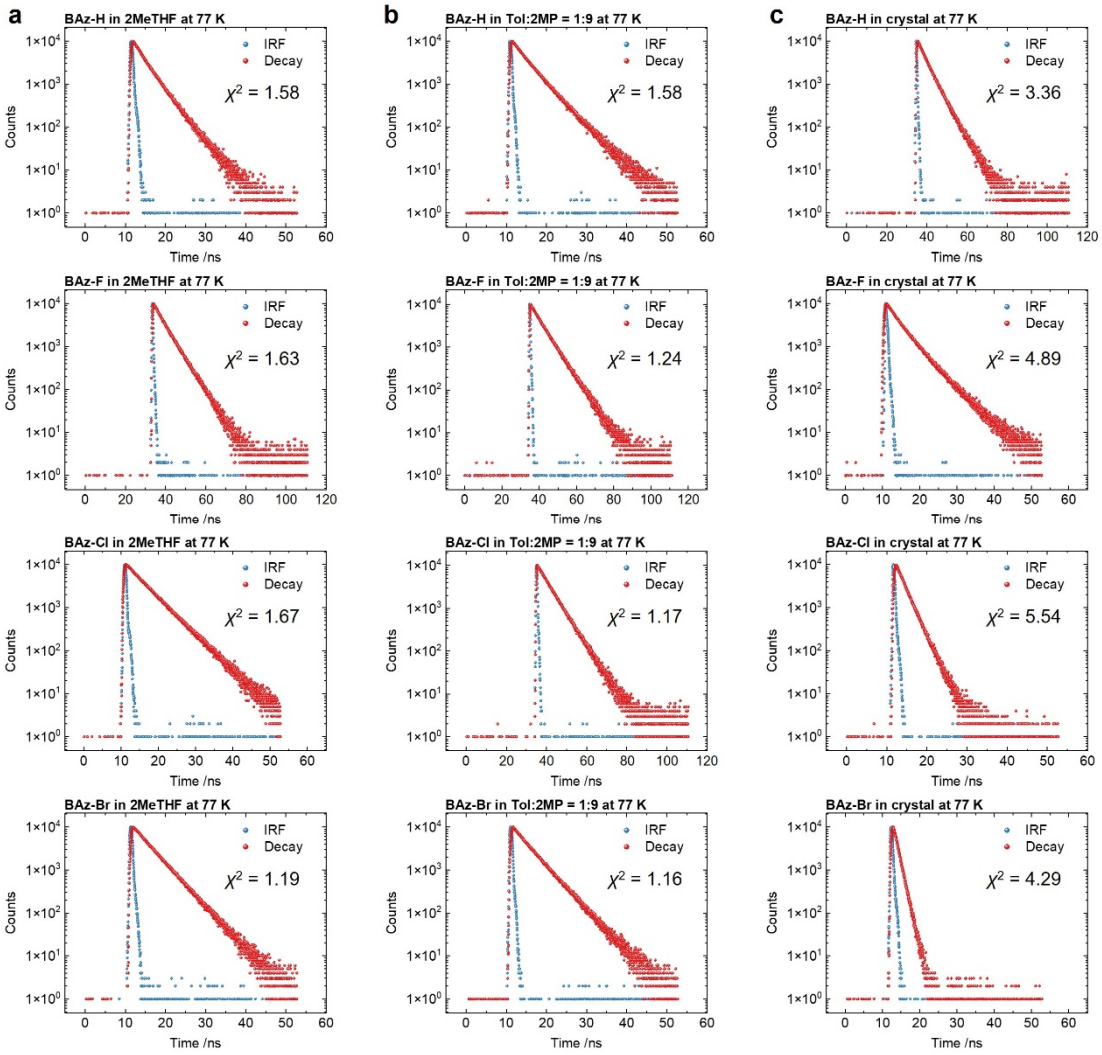

Figure S8. FL lifetime decay curves in (a) 2MeTHF (1.0×10^{-5} M), (b) toluene (Tol) and 2-methylpentane (2MP) (1/9, v/v) (1.0×10^{-5} M), and crystal at room temperature, excited at 369 nm with an LED laser. Their emissions at the FL peak tops were monitored.

Strickler–Berg (SB) equation

It should be noted that k_r is a function of the polarizability known as the Strickler–Berg (SB) equation (S1),[18–20]

$$k_{r,SB} = \frac{1}{\tau_0} = 2.880 \times 10^{-9}[\mathrm{cm^2 s^{-1}}] n^2 \frac{\int I(\tilde{\nu})\,\mathrm{d}\tilde{\nu}}{\int I(\tilde{\nu})\tilde{\nu}^{-3}\mathrm{d}\tilde{\nu}} \int \frac{\varepsilon_{\tilde{\nu}}}{\tilde{\nu}}\mathrm{d}\tilde{\nu} \qquad \text{(S1)}$$

τ_0 is the radiative lifetime (s), n is the refractive index of the environment, I is the fluorescence intensity, $\tilde{\nu}$ is the wavenumber ($\mathrm{cm^{-1}}$), and $\varepsilon_{\tilde{\nu}}$ is the molar extinction coefficient at a particular wavenumber $\tilde{\nu}$. Under the assumption of the band is sharp and the Stokes shift is negligible, $\tilde{\nu}$ is constant, and $\int I(\tilde{\nu})\,\mathrm{d}\tilde{\nu} / \int I(\tilde{\nu})\tilde{\nu}^{-3}\mathrm{d}\tilde{\nu}$ becomes $\tilde{\nu}^3$.[19] Therefore, the equation simplifies to equation (S2):

$$k_{r,SB} = 2.880 \times 10^{-9}[\mathrm{cm^2 s^{-1}}] n^2 \tilde{\nu}^2 \int \varepsilon_{\tilde{\nu}}\,\mathrm{d}\tilde{\nu} \qquad \text{(S2)}$$

The integral can be expressed through the oscillator strength (f) according to $f = 4.32 \times 10^{-9} \int \varepsilon_{\tilde{\nu}}\,\mathrm{d}\tilde{\nu}$ to obtain a common work form of the Strickler–Berg equation (1):

$$k_{r,SB} = 0.667[\mathrm{cm^2 s^{-1}}] n^2 \tilde{\nu}_{FL}^2 f \qquad \text{(1)}$$

$\tilde{\nu}_{FL}$ is the wavenumber ($\mathrm{cm^{-1}}$) of the fluorescence spectrum under the assumption that the band is sharp and the Stokes shift is negligible.

Computational details for theoretical calculation

The Gaussian 16 program package[21] was used for computation. The optimized geometry in the ground S_0 state of each molecule (**Opt**) were calculated with the density functional theory (DFT) at the B3LYP/6-311G(d,p) level. The resultant geometry was confirmed to be the local minima by performing frequency calculations and obtaining only positive frequencies. In addition, we extracted two geometries of the single molecule (**Monomer**) and the nearest neighbor dimer (**Dimer**) from each single crystal structure. Then, we calculated the S_0–S_1 transition energy of three geometries (**Opt**, **Monomer**, and **Dimer**) for each molecule with time-dependent DFT (TD-DFT) at TD-M06-2X/6-311+G(d,p) level. The molecular polarizability at 589 nm (α_{589}) was calculated by using the geometry of **Opt** at HF/6-311++G(2d,p) level.

The Q-Chem 6.1.0 program package[22] was used for computation of energy diagrams including both singlet (S_n) and triplet (T_n) states for evaluation of spin-orbit coupling (SOC) from S_n to T_n.

Results of theoretical calculation

Table S7. Results of representative transitions from TD-DFT calculations of BAz derivatives

		Energy gap / eV	Wavelength / nm	Oscillator Strength	transition	Assignment (Weight)
BAz-H	Opt	3.0061	412.44	0.4372	$S_0 \rightarrow S_1$	HOMO → LUMO (0.68443)
	Monomer	3.0863	401.72	0.4067	$S_0 \rightarrow S_1$	HOMO → LUMO (0.69302)
	Dimer	2.9640	418.30	0.0000	$S_0 \rightarrow S_1$	HOMO−1 → LUMO (0.36147)
						HOMO → LUMO (−0.11277)
						HOMO → LUMO+1 (0.57840)
		3.1289	396.26	0.6666	$S_0 \rightarrow S_2$	HOMO−1 → LUMO+1 (0.37497)
						HOMO → LUMO (−0.56121)
						HOMO → LUMO+1 (0.11144)
BAz-F	Opt	3.0567	405.61	0.5145	$S_0 \rightarrow S_1$	HOMO−4 → LUMO (−0.12612)
						HOMO → LUMO (0.68183)
	Monomer	3.2509	381.38	0.4698	$S_0 \rightarrow S_1$	HOMO → LUMO (0.69538)
	Dimer	3.1370	395.23	0.0000	$S_0 \rightarrow S_1$	HOMO−1 → LUMO (0.40108)
						HOMO → LUMO+1 (0.56998)
		3.2172	385.38	0.7310	$S_0 \rightarrow S_2$	HOMO−1 → LUMO+1 (0.30364)
						HOMO → LUMO (0.62515)
BAz-Cl	Opt	2.9628	418.47	0.6340	$S_0 \rightarrow S_1$	HOMO−4 → LUMO (−0.12790)
						HOMO → LUMO (0.68249)
	Monomer	3.0531	406.10	0.5989	$S_0 \rightarrow S_1$	HOMO → LUMO (0.68846)
	Dimer	2.9889	414.82	0.0000	$S_0 \rightarrow S_1$	HOMO−1 → LUMO (0.48726)
						HOMO−1 → LUMO+1 (0.10930)
						HOMO → LUMO (−0.12161)
						HOMO → LUMO+1 (0.46161)
		3.0664	404.33	1.0557	$S_0 \rightarrow S_2$	HOMO−1 → LUMO (0.12451)
						HOMO−1 → LUMO+1 (0.45129)
						HOMO → LUMO (0.48993)
						HOMO → LUMO+1 (−0.10916)
BAz-Br	Opt	2.9317	422.91	0.6963	$S_0 \rightarrow S_1$	HOMO−6 → LUMO (−0.13093)
						HOMO → LUMO (0.68044)
	Monomer	3.0341	408.64	0.6796	$S_0 \rightarrow S_1$	HOMO−6 → LUMO (0.10937)
						HOMO−1 → LUMO (−0.10193)
						HOMO → LUMO (0.68318)
	Dimer	2.9684	417.69	0.0008	$S_0 \rightarrow S_1$	HOMO−1 → LUMO (0.48655)
						HOMO → LUMO (−0.11561)
						HOMO → LUMO+1 (−0.46152)
		3.0457	407.08	1.1975	$S_0 \rightarrow S_2$	HOMO−1 → LUMO+1 (−0.45564)
						HOMO → LUMO (−0.49231)

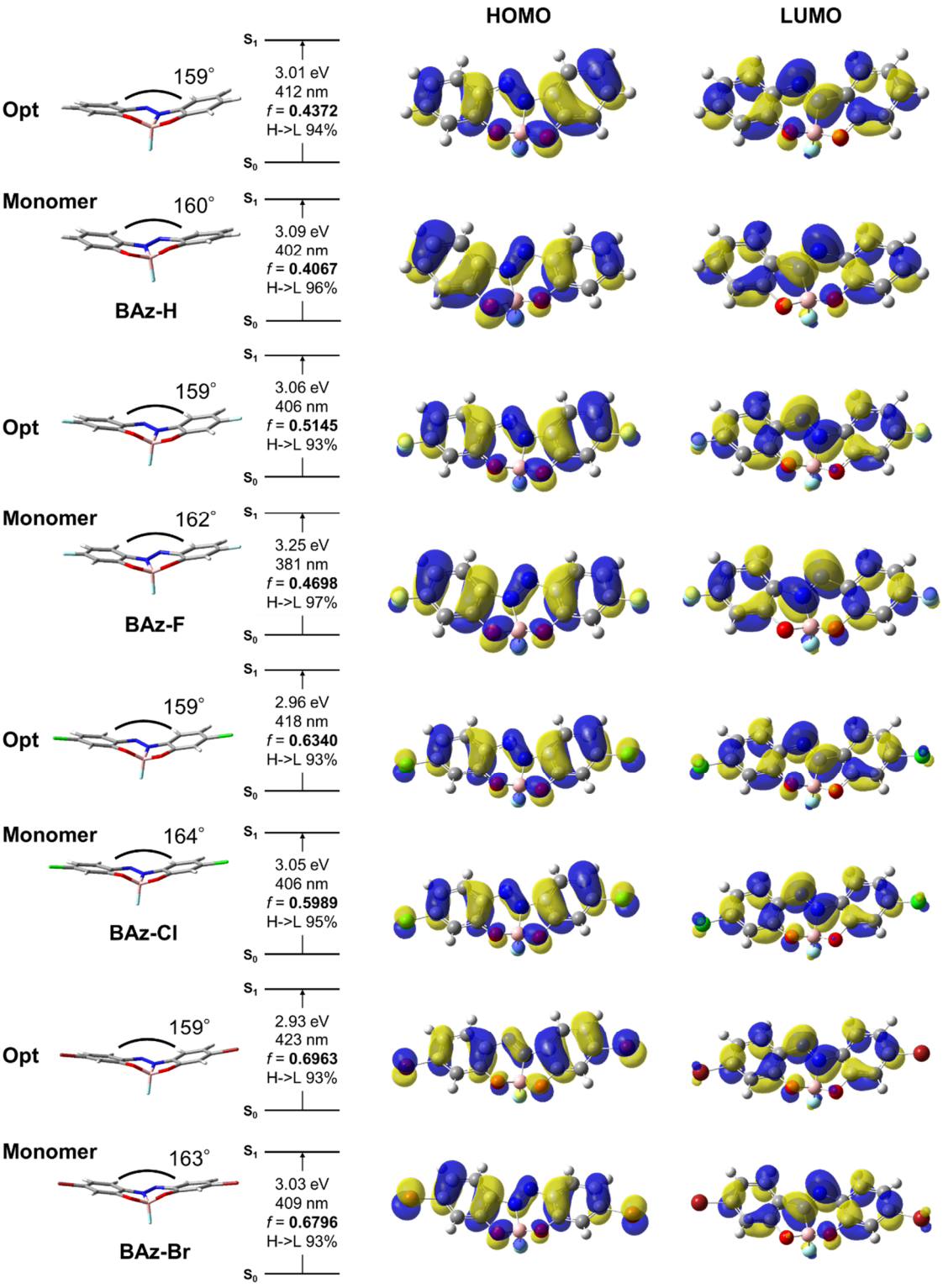

Figure S9. Molecular structures, representative transitions, and molecular orbital distributions of **Opt** and **Monomer** for BAz derivatives, obtained with TD-DFT calculations (isovalue = 0.03).

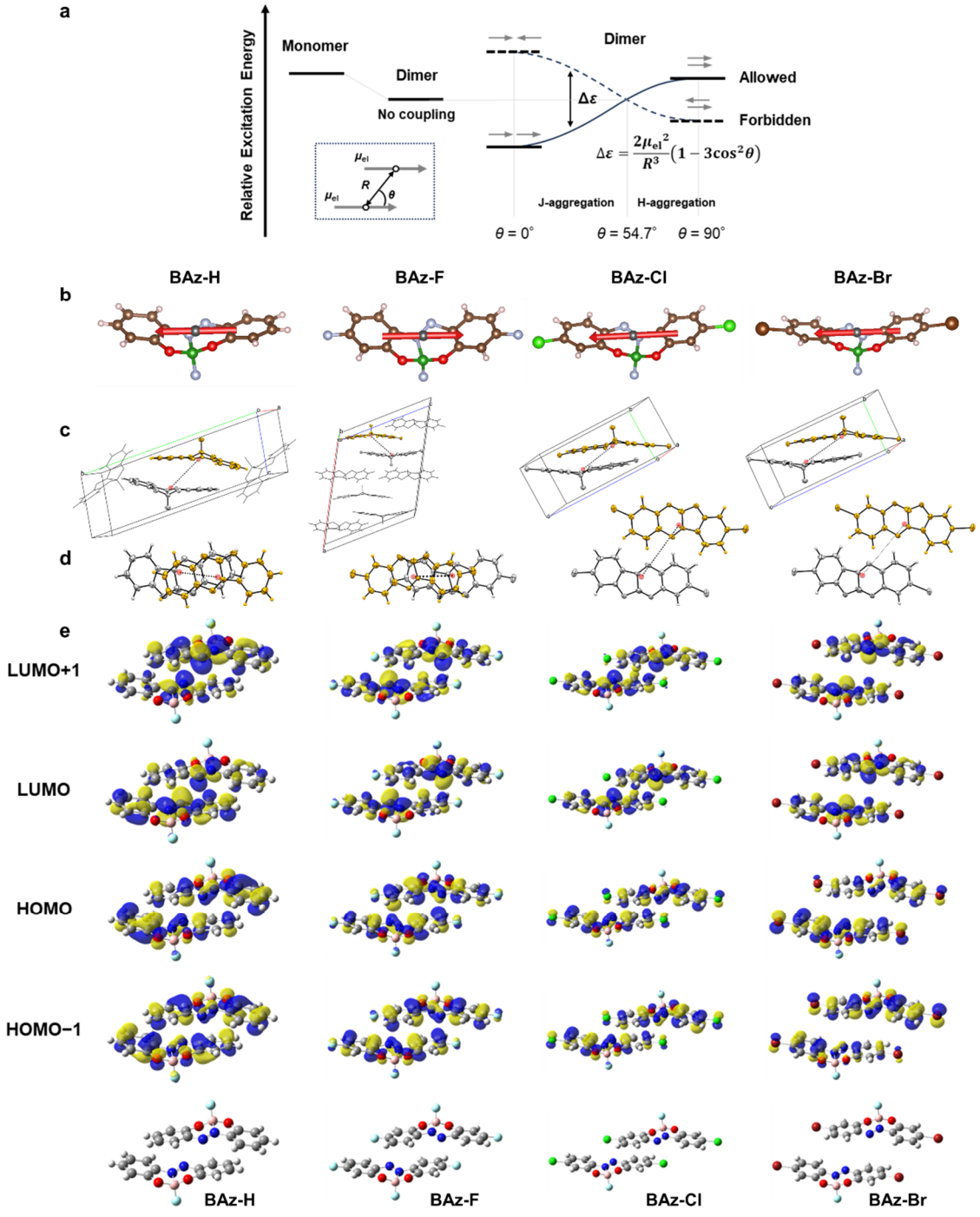

Figure S10. (a) Schematic representation of excitonic coupling. (b) The diagram of transition electric dipole moment (red vectors) and center of mass (gray sphere) for BAz derivatives, visualized with VESTA 3.[23] (c, d) Packing structures of (c) unit cell and (d) top view for BAz derivatives. "Ellipsoid" and "Wireframe" styles were used for the nearest neighbor dimer (**Dimer**) and other molecules, respectively, visualized Mercury.[9] (e) Molecular orbital distributions of **Dimer** for BAz derivatives, obtained with TD-DFT calculations (isovalue = 0.03).

Table S8. Dimer packing parameters and results of TD-DFT calculations in BAz derivatives

	R /Å	θ /°	$S_0 \rightarrow S_1$	$S_0 \rightarrow S_2$	$\Delta\varepsilon$ / eV
BAz-H	4.46	47	Forbidden	Allowed	0.16
BAz-F	5.20	39	Forbidden	Allowed	0.05
BAz-Cl	6.41	63	Forbidden	Allowed	0.08
BAz-Br	6.49	60	Forbidden	Allowed	0.08

IGMH analysis

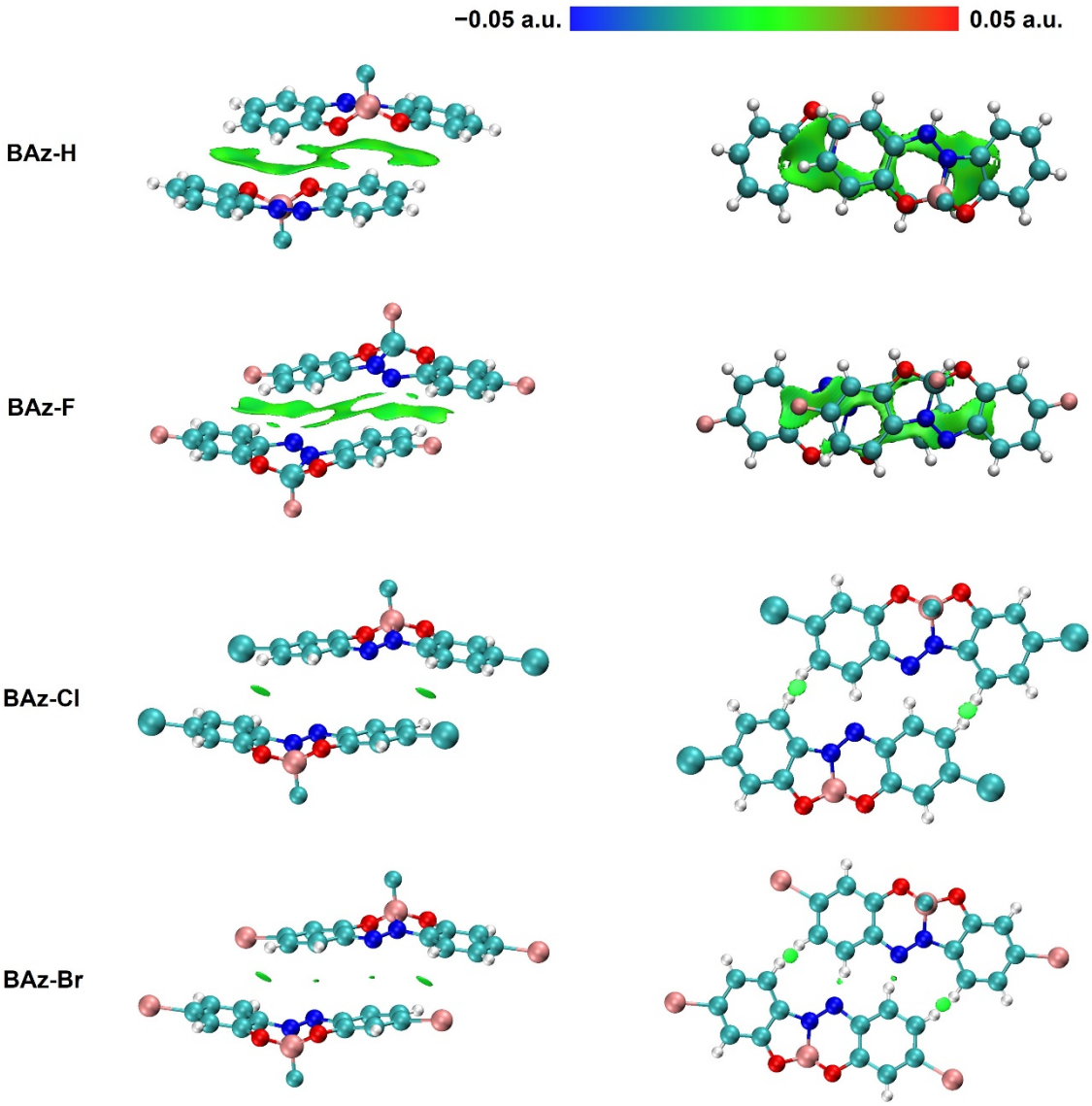

Figure S11. Sign(λ_2)ρ colored isosurfaces of δ_g^{inter} = 0.005 a.u. of the BAz derivatives corresponding to the IGMH analysis. In the interpretation of coloring method of mapped function sign(λ_2)ρ in the IGMH map from −0.05 to 0.05 a.u, the greenish area represents the existence of van der Waals interaction.[11]

Estimation of refractive index (*n*)

The refractive index at λ nm (n_λ) was estimated by Lorentz-Lorenz equation (S3):[24]

$$\frac{n_\lambda^2 - 1}{n_\lambda^2 + 2} = \frac{4\pi}{3}\frac{\rho \cdot N_\mathrm{A}}{M_\mathrm{w}}\alpha_\lambda = \frac{4\pi}{3}\frac{\alpha_\lambda}{V_\mathrm{mol}} \quad \text{(S3)}$$

ρ is the density (g cm^{-3}), N_A is the Abogadoro number (mol^{-1}), M_w is the molecular weight (g mol^{-1}), α_λ is the linear molecular polarizability at λ nm (cm^3), and V_mol is the molecular volume (cm^3). α_λ was simulated by the Gaussian 16 with "POLAR" and "CPHF= Rdfreq" keywords. In the crystal, we used ρ from the results of the single-crystal X-ray diffraction (SCXRD) analysis at 143 K. In the single molecule in vitrified solution, we estimated n_λ by using the molecular packing constant (K_p), and the van der Waals volume (V_vdw). K_p is defined as the equation (S4):

$$K_\mathrm{p} = \frac{V_\mathrm{vdw}}{V_\mathrm{mol}} \quad \text{(S4)}$$

From the equations (S3) and (S4), the n_λ was calculated by the equation (S5):

$$n_\lambda = \sqrt{\frac{1 + 2\varphi}{1 - \varphi}} \quad \text{(S5)}$$

$$\left(\varphi = \frac{4\pi}{3}\frac{\rho \cdot N_\mathrm{A}}{M_\mathrm{w}}\alpha_\lambda = \frac{4\pi}{3}\frac{K_\mathrm{p}}{V_\mathrm{vdw}}\alpha_\lambda\right)$$

In the vitrified solution, the molecules should form an amorphous state. Therefore, we used $K_\mathrm{p} = 0.68$, which is the value adopted in the typical amorphous polymer matrix.[25] V_vdw was calculated by using a molecular modeling software, Winmostar V11.[26] It is noted that n_λ depends on the wavelength. We calculated n_{589} because 589 nm is the wavelength of the sodium d-line, which is widely used as the standard value of the refractive index, and the emission bands from BAz derivatives were around 589 nm. To clarify the symbols, we defined them in the discussion as below; $n_{589} = n$, $\alpha_{589} = \alpha$.

Table S9. Calculated refractive index at 589 nm (n) in crystal from the equation (S5)

	ρ [a] / g cm^{-3}	N_A / mol^{-1}	M_w / g mol^{-1}	α / cm^3	n
BAz-H	1.515	6.022×10^{23}	242.01	3.35×10^{-23}	2.09
BAz-F	1.696	6.022×10^{23}	278.00	3.30×10^{-23}	2.03
BAz-Cl	1.680	6.022×10^{23}	310.90	4.09×10^{-23}	2.19
BAz-Br	2.072	6.022×10^{23}	399.82	4.50×10^{-23}	2.30

[a] from the single crystal structure analysis at 143 K.

Table S10. Calculated refractive index at 589 nm (n) in vitrified solution from the equation (S5)

	K_p	V_{vdw} / cm^3	α / cm^3	n
2MeTHF	0.68	8.69×10^{-23}	0.893×10^{-23}	1.50
Tol	0.68	9.45×10^{-23}	1.21×10^{-23}	1.65
2MP	0.68	10.24×10^{-23}	1.08×10^{-23}	1.51
Tol/2MP = 1/9 v/v	–	–	–	1.53 [a]

[a] n(Tol/2MP = 1/9 v/v) = 0.1×n(Tol) + 0.9×n(2MP)

Table S11. The calculated radiative constant ($k_{r,SB}$) from the equation (1) and related parameters

		$\tilde{\nu}_{FL}$ [a] /10^4 cm^{-1}	f [b] / molecule	n [c]	$k_{r,SB}$ /10^8 s^{-1}	($k_{r,SB}/n^2$) /10^8 s^{-1}
BAz-H	Opt	2.4253	0.4372	1.53 [d]	4.00	1.71
	Monomer	2.4893	0.4067	2.09	7.33	1.68
	Dimer	2.5236	0.3333	2.09	6.18	1.42
BAz-F	Opt	2.4654	0.5145	1.53 [d]	4.86	2.09
	Monomer	2.6221	0.4698	2.03	8.84	2.15
	Dimer	2.5948	0.3655	2.03	6.74	1.64
BAz-Cl	Opt	2.3897	0.634	1.53 [d]	5.63	2.41
	Monomer	2.4624	0.5989	2.19	11.6	2.42
	Dimer	2.4732	0.52785	2.19	10.3	2.15
BAz-Br	Opt	2.3646	0.6963	1.53 [d]	6.05	2.60
	Monomer	2.4471	0.6796	2.30	14.3	2.71
	Dimer	2.4565	0.59875	2.30	12.7	2.41

[a] The energy in the $S_0 \rightarrow S_1$ transition from Table S7; [b] The oscillator strength (f) from Table S7. For Dimer, f/2 value was used as an approximate value per molecule for comparison; [c] The calculated refractive index from Tables S9 and S10; [d] In vitrified solution (Tol/2MP = 1/9 v/v).

Table S12. The relationship among the measured radiative constant (k_r), the refractive index (n) [a], oscillator strength (f) [b], the energy of the emission ($\tilde{\nu}_{FL}$) [c]

		k_r /10^8 s^{-1}	(k_r/n^2) /10^8 s^{-1}	(k_r/f) /10^8 s^{-1}	($k_r/\tilde{\nu}_{FL}^2$) / cm^2 s^{-1}	($k_r/n^2 f\tilde{\nu}_{FL}^2$) / cm^2 s^{-1}
BAz-H	Tol/2MP = 1/9 v/v	0.63	0.27	1.4	0.22	0.22
	Crystal (Dimer)	0.55	0.13	1.7	0.20	0.14
BAz-F	Tol/2MP = 1/9 v/v	0.87	0.37	1.7	0.29	0.24
	Crystal (Dimer)	1.4	0.34	3.8	0.46	0.31
BAz-Cl	Tol/2MP = 1/9 v/v	1.0	0.43	1.6	0.35	0.23
	Crystal (Dimer)	1.7	0.35	3.2	0.67	0.26
BAz-Br	Tol/2MP = 1/9 v/v	1.2	0.51	1.7	0.42	0.26
	Crystal (Dimer)	1.9	0.36	3.2	0.76	0.24

[a] The calculated refractive index (n) at 589 nm from Tables S9 and S10; [b] The oscillator strength (f) from Table S7. For Dimer, f/2 value was used as an approximate value per molecule for comparison; [c] The energy of the emission ($\tilde{\nu}_{FL}$), $\tilde{\nu}_{FL} = 1/\lambda_{FL} \times 10^7$ from Table S6.

Energy diagrams of BAz derivatives including singlet (S_n) and triplet (T_n) states

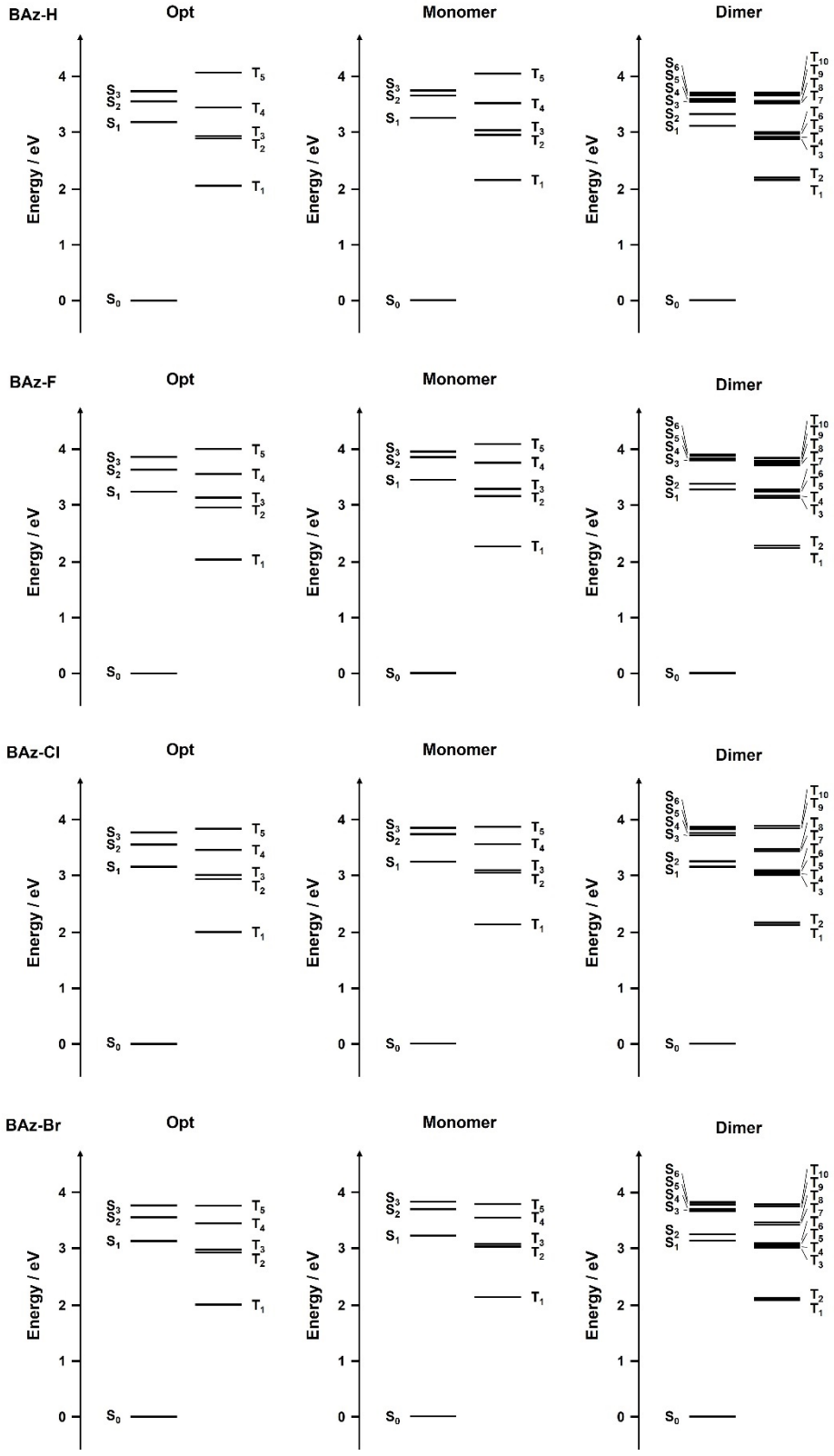

Figure S12. Energy diagrams of BAz derivatives at TDA-M06-2X/6-311+G(d,p) level with Q-Chem.[20]

Table S13. Spin-orbit coupling (SOC) (cm^{-1}) of $S_n \rightarrow T_n$ transitions in BAz derivatives

		T_1	T_2	T_3	T_4	T_5	T_6
BAz-H	Opt (S_1)	0.62	5.60	11.24	–	–	–
	Monomer (S_1)	0.42	4.54	10.77	–	–	–
	Dimer (S_1)	0.33	0.08	2.02	4.44	1.11	9.97
	Dimer (S_2)	0.10	0.40	4.97	2.25	10.17	1.09
BAz-F	Opt (S_1)	0.73	9.32	7.81	–	–	–
	Monomer (S_1)	1.10	8.88	8.12	–	–	–
	Dimer (S_1)	0.06	0.88	0.84	7.43	7.31	1.96
	Dimer (S_2)	0.96	0.06	7.59	0.85	2.01	7.52
BAz-Cl	Opt (S_1)	0.80	9.31	7.19	–	–	–
	Monomer (S_1)	0.19	6.33	10.48	–	–	–
	Dimer (S_1)	0.11	0.18	6.15	0.04	1.29	10.47
	Dimer (S_2)	0.23	0.15	0.02	5.67	10.23	1.30
BAz-Br	Opt (S_1)	2.10	11.17	6.28	–	–	–
	Monomer (S_1)	1.34	6.92	10.70	–	–	–
	Dimer (S_1)	0.71	0.75	6.05	2.80	1.30	10.91
	Dimer (S_2)	1.12	1.03	2.52	5.36	10.01	1.23

References

1 K. Suzuki, A. Kobayashi, S. Kaneko, K. Takehira, T. Yoshihara, H. Ishida, Y. Shiina, S. Oishi and S. Tobita, *Phys. Chem. Chem. Phys.*, 2009, **11**, 9850–9860.

2 Rigaku, REQAB. Program for Absorption Correction. Rigaku Corporation, Tokyo, Japan, 1998.

3 G. M. Sheldrick, *Acta Crystallogr. Sect. A: Found. Crystallogr.*, 2008, **64**, 112–122.

4 G. M. Sheldrick, *Acta Crystallogr. Sect. A: Found. Adv.*, 2015, **71**, 3–8.

5 G. M. Sheldrick, *Acta Crystallogr. Sect. C: Struct. Chem.*, 2015, **71**, 3–8.

6 G. M. Sheldrick, SHELXL-2018. Programs for Crystal Structure Analysis.; Universität Göttingen, Göttingen, Germany, 2018.

7 K. Wakita, Yadokari&XG. Program for Crystal Structure Analysis.; **2000**.

8 L. J. Farrugia, *ORTEP-3 for Windows-a version of ORTEP-III with a Graphical User Interface (GUI)*, *J. Appl. Cryst*., 1997, **30**, 565.

9 C. F. Macrae, I. Sovago, S. J. Cottrell, P. T. A. Galek, P. McCabe, E. Pidcock, M. Platings, G. P. Shields, J. S. Stevens, M. Towler and P. A. Wood, *J. Appl. Crystallogr.*, 2020, **53**, 226–235.

10 T. Lu and F. Chen, *J. Comput. Chem.*, 2012, **33**, 580–592.

11 T. Lu and Q. Chen, *J Comput Chem*, 2022, **43**, 539–555.

12 W. Humphrey, A. Dalke and K. Schulten, *J. Molec. Graphics*, 1996, **14**, 33–38.

13 A. B. Pangborn, M. A. Giardello, R. H. Grubbs, R. K. Rosen and F. J. Timmers, *Organometallics*, 1996, **15**, 1518–1520.

14 M. Gon, K. Tanaka and Y. Chujo, *Chem. – Eur. J.*, 2021, **27**, 7561–7571.

15 M. Gon, M. Yaegashi, K. Tanaka and Y. Chujo, *Chem. – Eur. J.*, 2023, **29**, e202203423.

16 M. Gon, K. Tanaka and Y. Chujo, *Angew. Chem. Int. Ed.*, 2018, **57**, 6546–6551.

17 G. Angulo, G. Grampp and A. Rosspeintner, *Spectrochim. Acta A: Mol. Biomol. Spectrosc.*, 2006, **65**, 727–731.

18 J. Shi, L. E. Aguilar Suarez, S.-J. Yoon, S. Varghese, C. Serpa, S. Y. Park, L. Lüer, D. Roca-Sanjuán, B. Milián-Medina and J. Gierschner, *J. Phys. Chem. C*, 2017, **121**, 23166–23183.

19 S. J. Strickler and R. A. Berg, *J. Chem. Phys.*, 1962, **37**, 814–822.

20 J. Mohanty and W. M. Nau, *Photochem. Photobiol. Sci.*, 2004, **3**, 1026–1031.

21 Gaussian 16, Revision C.01, M. J. Frisch, G. W. Trucks, H. B. Schlegel, G. E. Scuseria, M. A. Robb, J. R. Cheeseman, G. Scalmani, V. Barone, G. A. Petersson, H. Nakatsuji, X. Li, M. Caricato, A. V. Marenich, J. Bloino, B. G. Janesko, R. Gomperts, B. Mennucci, H. P. Hratchian, J. V. Ortiz, A. F. Izmaylov, J. L. Sonnenberg, D. Williams-Young, F. Ding, F. Lipparini, F. Egidi, J. Goings, B. Peng, A. Petrone, T. Henderson, D. Ranasinghe, V. G. Zakrzewski, J. Gao, N. Rega, G. Zheng, W. Liang, M. Hada, M. Ehara, K. Toyota, R. Fukuda, J. Hasegawa, M. Ishida, T. Nakajima, Y. Honda, O. Kitao, H. Nakai, T. Vreven, K. Throssell, J. A. Montgomery, Jr., J. E. Peralta, F. Ogliaro, M. J. Bearpark, J. J. Heyd, E. N. Brothers, K. N. Kudin, V. N. Staroverov, T. A. Keith, R. Kobayashi, J. Normand, K. Raghavachari, A. P. Rendell, J. C. Burant, S. S. Iyengar, J. Tomasi, M. Cossi, J. M.

Millam, M. Klene, C. Adamo, R. Cammi, J. W. Ochterski, R. L. Martin, K. Morokuma, O. Farkas, J. B. Foresman, and D. J. Fox, Gaussian, Inc., Wallingford CT, 2016.

22 E. Epifanovsky, A. T. B. Gilbert, X. Feng, J. Lee, Y. Mao, N. Mardirossian, P. Pokhilko, A. F. White, M. P. Coons, A. L. Dempwolff, Z. Gan, D. Hait, P. R. Horn, L. D. Jacobson, I. Kaliman, J. Kussmann, A. W. Lange, K. U. Lao, D. S. Levine, J. Liu, S. C. McKenzie, A. F. Morrison, K. D. Nanda, F. Plasser, D. R. Rehn, M. L. Vidal, Z.-Q. You, Y. Zhu, B. Alam, B. J. Albrecht, A. Aldossary, E. Alguire, J. H. Andersen, V. Athavale, D. Barton, K. Begam, A. Behn, N. Bellonzi, Y. A. Bernard, E. J. Berquist, H. G. A. Burton, A. Carreras, K. Carter-Fenk, R. Chakraborty, A. D. Chien, K. D. Closser, V. Cofer-Shabica, S. Dasgupta, M. de Wergifosse, J. Deng, M. Diedenhofen, H. Do, S. Ehlert, P.-T. Fang, S. Fatehi, Q. Feng, T. Friedhoff, J. Gayvert, Q. Ge, G. Gidofalvi, M. Goldey, J. Gomes, C. E. González-Espinoza, S. Gulania, A. O. Gunina, M. W. D. Hanson-Heine, P. H. P. Harbach, A. Hauser, M. F. Herbst, M. Hernández Vera, M. Hodecker, Z. C. Holden, S. Houck, X. Huang, K. Hui, B. C. Huynh, M. Ivanov, Á. Jász, H. Ji, H. Jiang, B. Kaduk, S. Kähler, K. Khistyaev, J. Kim, G. Kis, P. Klunzinger, Z. Koczor-Benda, J. H. Koh, D. Kosenkov, L. Koulias, T. Kowalczyk, C. M. Krauter, K. Kue, A. Kunitsa, T. Kus, I. Ladjánszki, A. Landau, K. V. Lawler, D. Lefrancois, S. Lehtola, R. R. Li, Y.-P. Li, J. Liang, M. Liebenthal, H.-H. Lin, Y.-S. Lin, F. Liu, K.-Y. Liu, M. Loipersberger, A. Luenser, A. Manjanath, P. Manohar, E. Mansoor, S. F. Manzer, S.-P. Mao, A. V. Marenich, T. Markovich, S. Mason, S. A. Maurer, P. F. McLaughlin, M. F. S. J. Menger, J.-M. Mewes, S. A. Mewes, P. Morgante, J. W. Mullinax, K. J. Oosterbaan, G. Paran, A. C. Paul, S. K. Paul, F. Pavošević, Z. Pei, S. Prager, E. I. Proynov, Á. Rák, E. Ramos-Cordoba, B. Rana, A. E. Rask, A. Rettig, R. M. Richard, F. Rob, E. Rossomme, T. Scheele, M. Scheurer, M. Schneider, N. Sergueev, S. M. Sharada, W. Skomorowski, D. W. Small, C. J. Stein, Y.-C. Su, E. J. Sundstrom, Z. Tao, J. Thirman, G. J. Tornai, T. Tsuchimochi, N. M. Tubman, S. P. Veccham, O. Vydrov, J. Wenzel, J. Witte, A. Yamada, K. Yao, S. Yeganeh, S. R. Yost, A. Zech, I. Y. Zhang, X. Zhang, Y. Zhang, D. Zuev, A. Aspuru-Guzik, A. T. Bell, N. A. Besley, K. B. Bravaya, B. R. Brooks, D. Casanova, J.-D. Chai, S. Coriani, C. J. Cramer, G. Cserey, A. E. DePrince III, R. A. DiStasio Jr, A. Dreuw, B. D. Dunietz, T. R. Furlani, W. A. Goddard III, S. Hammes-Schiffer, T. Head-Gordon, W. J. Hehre, C.-P. Hsu, T.-C. Jagau, Y. Jung, A. Klamt, J. Kong, D. S. Lambrecht, W. Z. Liang, N. J. Mayhall, C. W. McCurdy, J. B. Neaton, C. Ochsenfeld, J. A. Parkhill, R. Peverati, V. A. Rassolov, Y. Shao, L. V. Slipchenko, T. Stauch, R. P. Steele, J. E. Subotnik, A. J. W. Thom, A. Tkatchenko, D. G. Truhlar, T. Van Voorhis, T. A. Wesolowski, K. B. Whaley, H. L. Woodcock III, P. M. Zimmerman, S. Faraji, P. M. W. Gill, M. Head-Gordon, J. M. Herbert and A. I. Krylov, *J. Chem. Phys.*, 2021, **155**, 084801.

23 K. Momma and F. Izumi, *J. Appl. Crystallogr.*, 2011, **44**, 1272–1276.

24 N. Tanio and Y. Koike, *Jpn. J. Appl. Phys.*, 1997, **36**, 743–748.

25 S. Ando, *J. Photopolym. Sci. Technol.*, 2006, **19**, 351–360.

26 X-Ability Co. Ltd, Winmostar V11, Tokyo, Japan, 2023.

Cartesian coordinates for the optimized geometries

The structure of **BAz-H (Opt)** in S_0 geometry

C	4.392917	-0.04351	-0.50997
C	3.354724	-0.94876	-0.65157
C	2.048266	-0.5836	-0.30472
C	1.804613	0.757901	0.127631
C	2.878352	1.664669	0.244055
C	4.163558	1.266239	-0.05192
H	3.52374	-1.95923	-1.00209
H	2.650361	2.6748	0.561937
H	4.989353	1.959089	0.05004
N	0.524957	1.25852	0.266428
N	-0.37595	0.362989	0.277739
C	-1.73918	0.556894	0.102918
C	-2.27938	-0.71977	-0.18566
C	-2.51009	1.717995	0.103317
C	-3.63934	-0.83556	-0.46869
C	-3.86373	1.585056	-0.16919
H	-2.05515	2.677282	0.314999
C	-4.41238	0.321252	-0.45093
H	-4.06448	-1.80515	-0.69352
H	-4.50382	2.4585	-0.16673
O	1.058289	-1.46928	-0.44098
O	-1.38808	-1.71972	-0.18943
B	-0.12325	-1.21352	0.355872
F	0.061399	-1.56668	1.677526
H	5.401906	-0.35432	-0.7564
H	-5.47293	0.245336	-0.66286

The structure of **BAz-H (Monomer)** extracted from crystal structure

C	-0.303	13.725	3.979
C	0.673	14.693	3.69
C	0.332	15.783	2.91
H	0.976	16.445	2.687
C	-0.966	15.883	2.465

H	-1.216	16.633	1.939
C	-1.926	14.915	2.765
H	-2.815	15.021	2.447
C	-1.601	13.815	3.512
H	-2.241	13.14	3.701
C	1.026	10.737	5.377
C	2.389	11.068	5.308
C	3.338	10.099	5.587
H	4.264	10.294	5.495
C	2.929	8.849	5.999
H	3.579	8.193	6.22
C	1.579	8.534	6.098
H	1.315	7.671	6.394
C	0.638	9.458	5.773
H	-0.284	9.232	5.815
N	0.39	12.752	4.71
O	1.909	14.45	4.183
N	-0.016	11.559	4.905
O	2.792	12.301	4.915
B	1.814	13.326	5.106
F	1.754	13.756	6.425

The structure of **BAz-H (Dimer)** extracted from crystal structure

C	-0.303	13.725	3.979
C	0.673	14.693	3.69
C	0.332	15.783	2.91
H	0.976	16.445	2.687
C	-0.966	15.883	2.465
H	-1.216	16.633	1.939
C	-1.926	14.915	2.765
H	-2.815	15.021	2.447
C	-1.601	13.815	3.512
H	-2.241	13.14	3.701
C	1.026	10.737	5.377
C	2.389	11.068	5.308

C	3.338	10.099	5.587
H	4.264	10.294	5.495
C	2.929	8.849	5.999
H	3.579	8.193	6.22
C	1.579	8.534	6.098
H	1.315	7.671	6.394
C	0.638	9.458	5.773
H	-0.284	9.232	5.815
N	0.39	12.752	4.71
O	1.909	14.45	4.183
N	-0.016	11.559	4.905
O	2.792	12.301	4.915
B	1.814	13.326	5.106
F	1.754	13.756	6.425
C	4.003	7.72	3.106
C	3.026	6.752	3.395
C	3.368	5.662	4.175
H	2.723	5	4.398
C	4.665	5.562	4.619
H	4.915	4.812	5.146
C	5.626	6.53	4.319
H	6.514	6.424	4.637
C	5.3	7.63	3.573
H	5.941	8.305	3.383
C	2.673	10.708	1.707
C	1.31	10.377	1.777
C	0.361	11.346	1.498
H	-0.564	11.151	1.59
C	0.771	12.596	1.085
H	0.12	13.252	0.865
C	2.12	12.911	0.986
H	2.385	13.774	0.691
C	3.061	11.987	1.311
H	3.983	12.213	1.269
N	3.309	8.693	2.375

O	1.791	6.995	2.901
N	3.715	9.886	2.18
O	0.907	9.144	2.169
B	1.885	8.119	1.979
F	1.946	7.689	0.66

The structure of **BAz-F (Opt)** in S_0 geometry

C	4.375203	0.072717	-0.40111
C	3.379804	-0.8736	-0.54094
C	2.067548	-0.52835	-0.20664
C	1.789542	0.813857	0.21114
C	2.842289	1.74529	0.318384
C	4.139558	1.382644	0.033717
H	3.605548	-1.87676	-0.87624
H	2.593	2.754145	0.622465
H	4.965951	2.075304	0.117523
N	0.500526	1.286439	0.341727
N	-0.38083	0.370821	0.35675
C	-1.7468	0.53012	0.180079
C	-2.25668	-0.76322	-0.09974
C	-2.54883	1.669217	0.168087
C	-3.6101	-0.9227	-0.38252
C	-3.89865	1.508488	-0.10346
H	-2.12273	2.643165	0.370847
C	-4.38936	0.224382	-0.37082
H	-4.03716	-1.89081	-0.60421
H	-4.58305	2.345929	-0.11686
O	1.099615	-1.43504	-0.34036
O	-1.34303	-1.73863	-0.09561
B	-0.09139	-1.19713	0.45054
F	0.096344	-1.53585	1.773999
F	5.637738	-0.27856	-0.69504
F	-5.70256	0.09999	-0.63505

The structure of **BAz-F (Monomer)** extracted from crystal structure

C	2.61	4.517	8.562
C	2.169	3.265	8.119
C	2.064	3.022	6.765
H	1.744	2.192	6.433
C	2.44	4.03	5.922
C	2.882	5.28	6.324
H	3.133	5.942	5.689
C	2.945	5.528	7.672
H	3.213	6.381	7.992
C	2.088	4.681	12.06
C	1.512	3.443	12.387
C	0.988	3.255	13.663
H	0.579	2.437	13.917
C	1.09	4.309	14.536
C	1.671	5.516	14.239
H	1.731	6.201	14.894
C	2.16	5.708	12.98
H	2.546	6.541	12.738
N	2.52	4.257	9.935
N	2.473	5.214	10.775
O	1.833	2.348	9.055
F	2.399	3.787	4.59
O	1.436	2.473	11.448
F	0.58	4.143	15.786
F	3.589	2.211	10.581
B	2.34	2.715	10.354

The structure of **BAz-F (Dimer)** extracted from crystal structure

C	2.61	4.517	8.562
C	2.169	3.265	8.119
C	2.064	3.022	6.765
H	1.744	2.192	6.433
C	2.44	4.03	5.922
C	2.882	5.28	6.324
H	3.133	5.942	5.689

C	2.945	5.528	7.672
H	3.213	6.381	7.992
C	2.088	4.681	12.06
C	1.512	3.443	12.387
C	0.988	3.255	13.663
H	0.579	2.437	13.917
C	1.09	4.309	14.536
C	1.671	5.516	14.239
H	1.731	6.201	14.894
C	2.16	5.708	12.98
H	2.546	6.541	12.738
N	2.52	4.257	9.935
N	2.473	5.214	10.775
O	1.833	2.348	9.055
F	2.399	3.787	4.59
O	1.436	2.473	11.448
F	0.58	4.143	15.786
F	3.589	2.211	10.581
B	2.34	2.715	10.354
C	-1.133	4.714	7.659
C	-0.692	5.966	8.101
C	-0.587	6.209	9.456
H	-0.267	7.039	9.788
C	-0.963	5.201	10.298
C	-1.405	3.951	9.896
H	-1.656	3.289	10.531
C	-1.468	3.703	8.549
H	-1.736	2.85	8.228
C	-0.611	4.55	4.16
C	-0.035	5.788	3.833
C	0.489	5.976	2.557
H	0.898	6.794	2.303
C	0.387	4.922	1.684
C	-0.194	3.715	1.981
H	-0.254	3.03	1.326

C	-0.683	3.523	3.24
H	-1.069	2.69	3.482
N	-1.044	4.974	6.285
N	-0.996	4.017	5.445
O	-0.356	6.883	7.166
F	-0.922	5.444	11.63
O	0.041	6.758	4.772
F	0.897	5.088	0.435
F	-2.112	7.02	5.639
B	-0.863	6.516	5.867

The structure of **BAz-Cl (Opt)** in S_0 geometry

C	4.389231	0.148949	-0.31484
C	3.39549	-0.80656	-0.43331
C	2.077749	-0.47233	-0.10334
C	1.781242	0.872157	0.286647
C	2.822683	1.817288	0.376253
C	4.124004	1.465478	0.098216
H	3.613811	-1.8172	-0.74956
H	2.563292	2.829388	0.661217
H	4.929589	2.182206	0.175032
N	0.485951	1.32967	0.406673
N	-0.38189	0.401152	0.439214
C	-1.74867	0.53753	0.254484
C	-2.2397	-0.76695	0.002409
C	-2.56744	1.663419	0.214847
C	-3.59054	-0.9514	-0.28195
C	-3.91366	1.477086	-0.05729
H	-2.15842	2.648808	0.397207
C	-4.39744	0.180597	-0.30001
H	-3.98519	-1.93768	-0.48073
H	-4.59512	2.31579	-0.08684
O	1.124568	-1.39723	-0.21812
O	-1.31392	-1.7308	0.030659
B	-0.07064	-1.16168	0.56709

F	0.120204	-1.46851	1.896987
Cl	6.039415	-0.29539	-0.68992
Cl	-6.10458	-0.01517	-0.64531

The structure of **BAz-Cl (Monomer)** extracted from crystal structure

C	0.644	2.588	2.725
C	-0.295	2.47	1.695
C	0.085	1.926	0.472
H	-0.529	1.814	-0.218
C	1.401	1.561	0.323
C	2.344	1.684	1.354
H	3.224	1.418	1.217
C	1.96	2.2	2.567
H	2.57	2.286	3.265
C	-0.809	3.403	5.862
C	-2.169	3.446	5.481
C	-3.146	3.592	6.456
H	-4.047	3.6	6.225
C	-2.76	3.723	7.767
C	-1.43	3.684	8.166
H	-1.202	3.771	9.064
C	-0.463	3.515	7.215
H	0.431	3.473	7.468
N	-0.104	3.139	3.802
N	0.261	3.1	5.023
O	-1.565	2.916	1.965
O	-2.515	3.239	4.2
B	-1.511	3.625	3.245
F	-1.475	4.994	3.066
Cl	1.915	0.922	-1.197
Cl	-3.982	3.95	8.984

The structure of **BAz-Cl (Dimer)** extracted from crystal structure

C	0.644	2.588	2.725
C	-0.295	2.47	1.695

C	0.085	1.926	0.472
H	-0.529	1.814	-0.218
C	1.401	1.561	0.323
C	2.344	1.684	1.354
H	3.224	1.418	1.217
C	1.96	2.2	2.567
H	2.57	2.286	3.265
C	-0.809	3.403	5.862
C	-2.169	3.446	5.481
C	-3.146	3.592	6.456
H	-4.047	3.6	6.225
C	-2.76	3.723	7.767
C	-1.43	3.684	8.166
H	-1.202	3.771	9.064
C	-0.463	3.515	7.215
H	0.431	3.473	7.468
N	-0.104	3.139	3.802
N	0.261	3.1	5.023
O	-1.565	2.916	1.965
O	-2.515	3.239	4.2
B	-1.511	3.625	3.245
F	-1.475	4.994	3.066
Cl	1.915	0.922	-1.197
Cl	-3.982	3.95	8.984
C	-5.718	1.252	10.724
C	-4.779	1.37	11.755
C	-5.159	1.914	12.977
H	-4.545	2.026	13.667
C	-6.475	2.279	13.126
C	-7.418	2.156	12.095
H	-8.298	2.423	12.232
C	-7.034	1.64	10.882
H	-7.644	1.555	10.184
C	-4.265	0.437	7.587
C	-2.905	0.394	7.969

C	-1.928	0.248	6.994
H	-1.027	0.24	7.224
C	-2.314	0.117	5.682
C	-3.644	0.156	5.283
H	-3.872	0.069	4.385
C	-4.611	0.326	6.234
H	-5.505	0.367	5.981
N	-4.97	0.702	9.647
N	-5.335	0.74	8.426
O	-3.509	0.924	11.484
O	-2.559	0.601	9.249
B	-3.563	0.215	10.204
F	-3.599	-1.154	10.383
Cl	-6.989	2.918	14.646
Cl	-1.092	-0.11	4.466

The structure of **BAz-Br (Opt)** in S_0 geometry

C	-3.41159	0.74013	-0.26494
C	-2.08928	0.408322	0.052537
C	-1.77744	-0.94607	0.392847
C	-2.80853	-1.90514	0.44893
C	-4.1145	-1.55821	0.184856
C	-4.39461	-0.23012	-0.18036
H	-3.63584	1.760278	-0.54419
H	-2.53766	-2.92412	0.696807
H	-4.90871	-2.28947	0.237931
N	-0.47735	-1.39345	0.494869
N	0.380607	-0.45704	0.560268
C	1.748305	-0.5719	0.3688
C	2.22476	0.746103	0.164217
C	2.579153	-1.6866	0.286681
C	3.573677	0.955978	-0.11493
C	3.923448	-1.47619	0.019854
H	2.181019	-2.68248	0.433355
C	4.392748	-0.16606	-0.17564

H	3.952199	1.955147	-0.2771
H	4.609921	-2.30899	-0.0404
B	0.0526	1.096234	0.745746
F	-0.13934	1.352328	2.086403
Br	-6.20039	0.249319	-0.5704
Br	6.251701	0.081106	-0.54663
O	-1.14653	1.347305	-0.0289
O	1.28836	1.698278	0.22894

The structure of **BAz-Br (Monomer)** extracted from crystal structure

C	1.221	1.456	11.099
C	2.169	1.535	12.119
C	1.824	2.067	13.348
H	2.443	2.132	14.039
C	0.529	2.497	13.506
C	-0.432	2.416	12.506
H	-1.3	2.71	12.664
C	-0.086	1.893	11.276
H	-0.708	1.836	10.588
C	2.584	0.607	7.944
C	3.958	0.548	8.293
C	4.911	0.387	7.299
H	5.817	0.367	7.508
C	4.482	0.256	5.99
C	3.137	0.311	5.637
H	2.878	0.221	4.749
C	2.212	0.498	6.61
H	1.312	0.553	6.381
N	1.931	0.889	10.016
N	1.54	0.929	8.807
O	3.417	1.097	11.793
O	4.352	0.694	9.576
B	3.342	0.36	10.541
F	3.246	-0.997	10.741
Br	0.024	3.209	15.186

Br	5.759	-0.034	4.625

The structure of **BAz-Br (Dimer)** extracted from crystal structure

C	1.221	1.456	11.099
C	2.169	1.535	12.119
C	1.824	2.067	13.348
H	2.443	2.132	14.039
C	0.529	2.497	13.506
C	-0.432	2.416	12.506
H	-1.3	2.71	12.664
C	-0.086	1.893	11.276
H	-0.708	1.836	10.588
C	2.584	0.607	7.944
C	3.958	0.548	8.293
C	4.911	0.387	7.299
H	5.817	0.367	7.508
C	4.482	0.256	5.99
C	3.137	0.311	5.637
H	2.878	0.221	4.749
C	2.212	0.498	6.61
H	1.312	0.553	6.381
N	1.931	0.889	10.016
N	1.54	0.929	8.807
O	3.417	1.097	11.793
O	4.352	0.694	9.576
B	3.342	0.36	10.541
F	3.246	-0.997	10.741
Br	0.024	3.209	15.186
Br	5.759	-0.034	4.625
C	0.609	2.718	2.86
C	-0.339	2.64	1.84
C	0.005	2.107	0.611
H	-0.614	2.042	-0.079
C	1.301	1.677	0.454
C	2.262	1.759	1.453

H	3.13	1.464	1.295
C	1.915	2.281	2.683
H	2.538	2.339	3.371
C	-0.754	3.568	6.015
C	-2.128	3.627	5.666
C	-3.082	3.788	6.66
H	-3.987	3.807	6.451
C	-2.652	3.918	7.969
C	-1.308	3.863	8.323
H	-1.048	3.953	9.21
C	-0.382	3.677	7.35
H	0.517	3.621	7.579
N	-0.102	3.285	3.944
N	0.289	3.245	5.152
O	-1.587	3.078	2.166
O	-2.522	3.48	4.384
B	-1.512	3.814	3.419
F	-1.417	5.171	3.218
Br	1.805	0.965	-1.227
Br	-3.929	4.208	9.334

The structure of **2-methylterahydrofran (2MeTHF) (Opt)** in S_0 geometry

C	1.361	-0.843	0.173
H	1.599	-1.107	1.21
H	1.983	-1.459	-0.485
C	1.543	0.662	-0.081
C	0.126	1.202	0.15
H	2.291	1.111	0.575
H	1.851	0.844	-1.115
H	-0.063	2.154	-0.351
C	-0.739	0.062	-0.399
H	-0.069	1.332	1.22
O	-0.022	-1.139	-0.067
C	-2.145	-0.036	0.166
H	-0.794	0.147	-1.496

H	-2.112	-0.113	1.256
H	-2.735	0.844	-0.107
H	-2.651	-0.922	-0.223

The structure of **Toluene (Tol) (Opt)** in S_0 geometry

C	0.91224295	0.00611941	-0.00001357
C	2.42227328	0.00229841	0.00001289
C	0.19734018	-1.19801465	-0.00001032
C	0.19001372	1.20239469	-0.00001403
C	-1.2042109	1.20030848	0.00001978
C	-1.19414	-1.20582129	0.00000706
C	-1.90155821	-0.00427484	-0.00000239
H	0.72514285	2.14654479	-0.00001994
H	-1.74417228	2.1407655	-0.00001973
H	0.73889436	-2.13900702	-0.00002912
H	-1.72789847	-2.14987339	0.00001712
H	-2.98561368	-0.00857935	0.00000436
H	2.81905541	-0.51273846	0.88046759
H	2.81907524	-0.51277641	-0.88040906
H	2.82375039	1.01760303	-0.00000776

The structure of **2-methylpentane (2MP) (Opt)** in S_0 geometry

C	-2.84516341	-0.21228135	0.15003106
H	-2.99502529	-1.22627675	-0.23388287
C	-1.49835877	0.35902935	-0.30453532
H	-3.6790387	0.40217628	-0.20044934
H	-2.90523633	-0.2613759	1.24184918
C	-0.30495914	-0.48021706	0.16870018
H	-1.48082908	0.42281295	-1.39964724
H	-1.40368307	1.38629486	0.06253721
H	-0.29306411	-0.50737184	1.26730539
H	-0.45926919	-1.51707086	-0.1564938
C	1.07461674	-0.01304252	-0.33292933
H	1.02558708	0.04469509	-1.42925946
C	1.45314496	1.3783825	0.19495031

C	2.15661451	-1.03895131	0.03261386
H	2.24577315	-1.14111132	1.11980943
H	1.92401686	-2.0268215	-0.37587864
H	3.13545481	-0.73882679	-0.35290148
H	0.74043394	2.14552944	-0.11677779
H	1.48968752	1.38068618	1.29024111